immune responses such as CHS, it is of great interest to understand how IL-1 modulates the recognition of antigen by skin T cells.

Using a mouse CHS model, here we examined how DCs and effector T cells encounter each other efficiently in the skin. We found that upon encountering antigenic stimuli, dDCs formed clusters in which effector T cells were activated and proliferated in an antigen-dependent manner. These DC–T cell clusters were initiated by skin macrophages via IL-1R signaling and were essential for the establishment of cutaneous acquired immune responses.

RESULTS

Formation of DC–T cell clusters at antigen-challenged sites

To explore the accumulation of cells of the immune system in the skin, we examined the clinical and histological features of the elicitation of human allergic contact dermatitis. Allergic contact dermatitis is the most common of eczematous skin diseases, affecting 15–20% of the general population worldwide[8], and is mediated by T cells. Although antigens should be spread evenly over the surface of skin, clinical manifestations commonly include discretely distributed small vesicles (**Fig. 1a**), which suggests an uneven occurrence of intense inflammation. Histological examination of allergic contact dermatitis showed spongiosis, intercellular edema in the epidermis and colocalization of perivascular infiltrates of $CD3^+$ T cells and spotty accumulation of $CD11c^+$ DCs in the dermis, especially beneath the vesicles (**Fig. 1b**). These findings led us to hypothesize that focal accumulation of T cells and DCs in the dermis might contribute to vesicle formation in early eczema.

To characterize the DC–T cell clusters in elicitation reactions, we used two-photon microscopy to obtain time-lapse images in a mouse model of CHS. We isolated T cells from the draining LNs of mice sensitized with the hapten DNFB (2,4-dinitrofluorobenzene), labeled the cells with fluorescent dye and transferred them into mice that express the common DC marker CD11c tagged with yellow fluorescent protein (YFP). In the steady state, YFP^+ dDCs distributed diffusely (**Fig. 1c**), representative of nondirected movement in a random fashion (**Supplementary Fig. 1**), as reported before[9]. After topical challenge with DNFB, YFP^+ dDCs transiently increased their velocity and formed clusters in the dermis, with the clusters becoming larger and more evident after 24 h (**Fig. 1c** and **Supplementary Movie 1**). At the same time, transferred T cells accumulated in the DC clusters and interacted with YFP^+ DCs for several hours (**Fig. 1d** and **Supplementary Movie 2**). Thus, we observed accumulation of DCs and T cells in the dermis in mice during CHS responses. We noted that the intercellular spaces between keratinocytes overlying the DC–T cell clusters in the dermis were enlarged (**Fig. 1e**), which replicated observations made for human allergic contact dermatitis (**Fig. 1b**).

We next sought to determine which of the two main DC populations in skin, epidermal LCs or dDCs, was essential for the elicitation of CHS. To deplete mice of all cutaneous DC subsets, we used mice with sequence expressing the diphtheria toxin receptor (DTR) under the control of the promoter of the gene encoding langerin as recipients (in such 'Langerin-DTR' mice, treatment with diphtheria toxin (DT) leads to depletion of langerin-positive cells) and mice that express a transgene encoding DTR under the control of promoter of the gene encoding CD11c as donors (in such 'CD11c-DTR' mice, treatment with DT leads to transient depletion of $CD11c^+$ DC populations). To selectively deplete mice of LCs or dDCs, we transferred bone marrow (BM) cells from C57BL/6 mice or CD11c-DTR mice into Langerin-DTR or C57BL/6 mice, respectively (**Supplementary Fig. 2a,b**). We injected DT into the chimeras to ensure depletion of each DC subset before elicitation and found that ear swelling and inflammatory histological findings were significantly attenuated in the absence of dDCs but not in the absence of LCs (**Fig. 1f** and **Supplementary Fig. 2c**). In addition, production of interferon-γ (IFN-γ) in skin T cells was substantially suppressed in mice depleted of dDCs (**Fig. 1g**). These results suggested that dDCs, not epidermal LCs, were essential for T cell activation and the elicitation of CHS responses.

Antigen-dependent proliferation of skin effector T cells *in situ*

To evaluate the effect of DC–T cell clusters in the dermis, we determined whether T cells had acquired the ability to proliferate via the accumulation of DC–T cell clusters in the dermis. We purified $CD4^+$ or $CD8^+$ T cells from the draining LNs of DNFB-sensitized mice, labeled

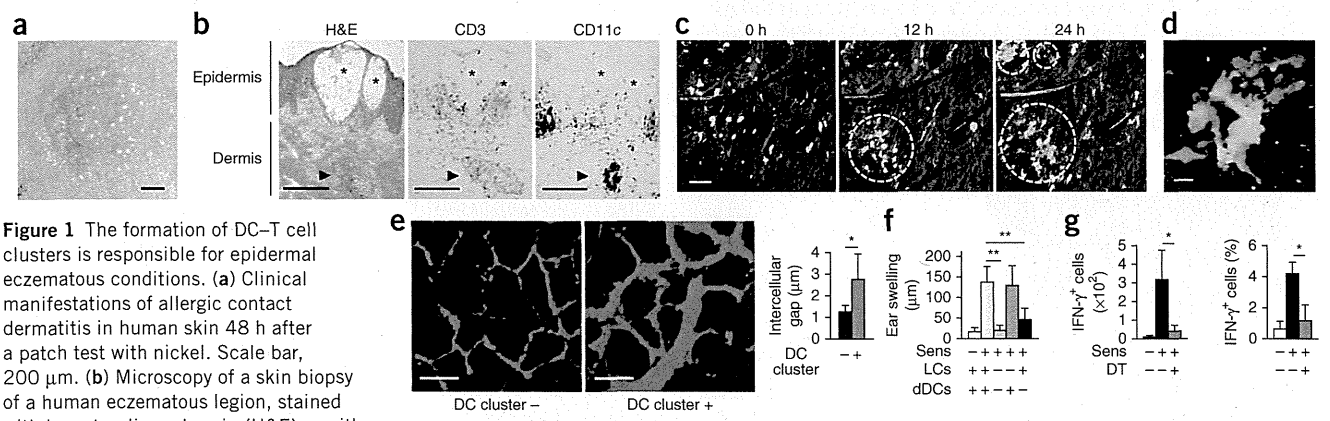

Figure 1 The formation of DC–T cell clusters is responsible for epidermal eczematous conditions. (**a**) Clinical manifestations of allergic contact dermatitis in human skin 48 h after a patch test with nickel. Scale bar, 200 μm. (**b**) Microscopy of a skin biopsy of a human eczematous legion, stained with hematoxylin and eosin (H&E) or with antibody to CD3 (anti-CD3) or anti-CD11c. *, epidermal vesicles; arrowheads indicate dDC–T cell clusters. Scale bars, 250 μm. (**c**) Sequential images of leukocyte clusters in the elicitation phase of CHS. White outlined areas indicate dermal accumulation of DCs (green) and T cells (red). Scale bar, 100 μm. (**d**) Enlargement of DC–T cell cluster in **c**. Scale bar, 10 μm. (**e**) Intercellular edema of the epidermis overlying a DC–T cell cluster in the dermis, with keratinocytes (red) visualized with isolectin B4 (left), and distance between adjacent keratinocytes above (+) or not above (–) a DC–T cell cluster ($n = 20$ images per condition) (right). Scale bars, 10 μm. (**f**) Ear swelling 24 h after CHS with (+) or without (–) sensitization (Sens) and with (–) or without (+) subset-specific depletion of DCs ($n = 5$ mice per group). (**g**) Quantification (left) and frequency (right) of IFN-γ-producing T cells in the ear 18 h after CHS with or without sensitization (as in **f**) and with (DT +) or without (DT –) depletion of dDCs ($n = 5$ mice per group). $^*P < 0.05$ and $^{**}P < 0.001$ (unpaired Student's *t*-test). Data are representative of five independent experiments (**a–d**) or three experiments (**f,g**) or are pooled from three experiments (**e**; error bars (**e–g**), s.d.).

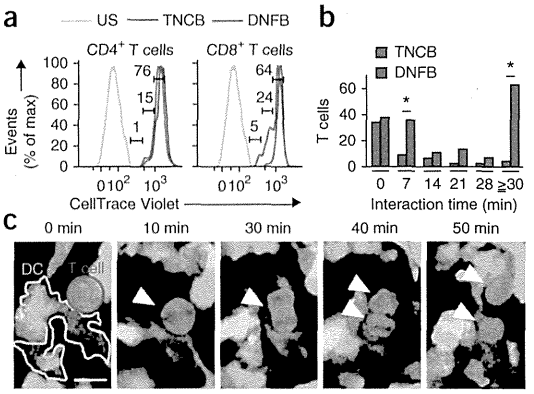

Figure 2 Antigen-dependent T cell proliferation in DC–T cell clusters. (**a**) Proliferation CD4+ T cells (left) or CD8+ T cells (right) in the skin of recipient mice 24 h after transfer of CellTrace Violet–labeled cells from donor mice left unsensitized (US) or sensitized with DNFB or TNCB, assessed as dilution of tracer in the challenged sites. Numbers adjacent to bracketed lines indicate percent cells that had proliferated. (**b**) Conjugation time of dDCs with T cells sensitized with DNFB ($n = 160$ T cells) or TNCB ($n = 60$ T cells), assessed at 24 h after challenge with DNFB. $^*P < 0.05$ (unpaired Student's *t*-test). (**c**) Sequential images of dividing T cells (red) in DC–T cell clusters. Green, dDCs; arrowheads indicate a dividing T cell. Data are representative of three experiments.

the cells with a division-tracking dye and transferred the cells into naive mice. Twenty-four hours after the application of DNFB to the recipient mice, we collected the skin to evaluate T cell proliferation by dilution of fluorescence intensity. Most of the infiltrating T cells (>90%) were CD44+CD62L− effector T cells (**Supplementary Fig. 2d**). Among the infiltrating T cells, CD8+ T cells proliferated actively, whereas the CD4+ T cells showed low proliferative potency (**Fig. 2a**). This T cell proliferation was antigen dependent because T cells sensitized with the hapten TNCB (2,4,6-trinitrochlorobenzene) exhibited low proliferative activity in response to the application of DNFB (**Fig. 2a**). In line with that finding, the DC–T cell conjugation time was prolonged in the presence of the cognate antigen DNFB (**Fig. 2b**), and the T cells interacting with DCs within DC–T cell clusters proliferated (**Fig. 2c** and **Supplementary Movie 3**). These findings indicated that skin effector T cells conjugated with DCs and proliferated *in situ* in an antigen-dependent manner.

LFA-1-dependent activation of CD8+ T cells in DC–T cell clusters

Sustained interaction between DCs and naive T cells, known as the 'immunological synapse', is maintained by cell adhesion molecules[10]. In particular, the integrin LFA-1 (CD58) on T cells binds to cell-surface glycoproteins, such as the intercellular adhesion molecule ICAM-1, on APCs, which is essential for the proliferation and activation of naive T cells during antigen recognition in the LNs. To determine whether LFA-1–ICAM-1 interactions are required for the activation of effector T cells in DC–T cell clusters in the skin, we elicited a CHS response in mouse ear skin with DNFB, then injected KBA, a neutralizing antibody to LFA-1, intravenously 14 h later. Such administration of KBA reduced the accumulation of T cells in the dermis (**Fig. 3a**). The velocity of T cells in the cluster was 0.65 ± 0.29 μm/min (mean ± s.d.) at 14 h after the DNFB challenge and increased up to threefold (1.64 ± 1.54 μm/min) at 8 h after treatment with KBA, while it was not affected by treatment with the isotype-matched control antibody immunoglobulin G (IgG) (**Fig. 3b**). At the outside of clusters, T cells smoothly migrated at the mean velocity of 2.95 ± 1.19 μm/min, consistent with published results[11], and this was not affected by treatment with the control antibody IgG (data not shown). Treatment with KBA also significantly attenuated ear swelling (**Fig. 3c**) as well as IFN-γ production by skin CD8+ T cells (**Fig. 3d,e**). These results suggested that the DC–effector T cell conjugates were integrin dependent, similar to the DC–naive T cell interactions in draining LNs.

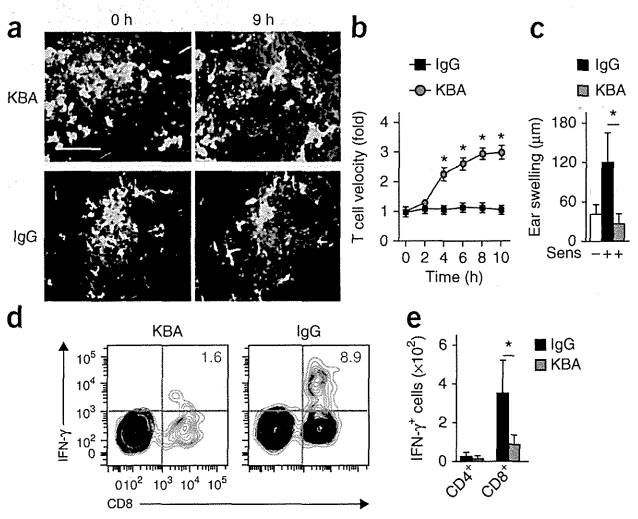

Figure 3 LFA-1 is essential for the persistence of DC–T cell clustering and for T cell activation in the skin. (**a**) Clusters of DCs (green) and T cells (red) in the DNFB-challenged site before (0 h) and 9 h after treatment with KBA (LFA-1-neutralizing antibody) or IgG (isotype-matched control antibody). Scale bar, 100 μm. (**b**) T cell velocity in DNFB-challenged sites at various times (horizontal axis) after treatment with KBA or IgG ($n = 30$ T cells per group), presented relative to velocity at time 0, set as 1. (**c**) Ear swelling 24 h after treatment with KBA or IgG in mice ($n = 5$ per group) left unsensitized (Sens –) or challenged with DNFB (Sens +). (**d,e**) IFN-γ production by CD8+ T cells (**d**) and quantification of IFN-γ-producing cells in the CD4+ or CD8+ population (**e**) in skin from mice ($n = 5$ per group) challenged with DNFB, then treated with KBA or IgG 12 h later, assessed 6 h after antibody treatment. Numbers in top right quadrants (**d**) indicate percent IFN-γ+CD8+ T cells. $^*P < 0.05$ (unpaired Student's *t*-test). Data are representative of three experiments (error bars (**b,c,e**), s.d.).

dDC clustering requires skin macrophages

We next examined the factors that initiated the accumulation of DC–T cell clusters. dDC clusters also formed in response to the initial application of hapten (sensitization phase), but their number decreased significantly 48 h after sensitization, while DC clusters persisted for 48 h in the elicitation phase (**Fig. 4a** and **Supplementary Fig. 3a**). These DC clusters were abrogated 7 d after application of DNFB (data not shown). These observations suggested that the accumulation of DC–T cell clusters was initiated by DC clustering, which then induced the accumulation, proliferation and activation of T cells, a process that depended on the presence of antigen-specific effector T cells *in situ*. DC clusters were also induced by solvents (such as acetone) or adjuvants (such as dibutylphthalic acid) and by pathogenic inoculation with *Mycobacterium bovis* bacillus Calmette-Guérin (**Supplementary Fig. 3b,c**). In addition, we observed DC clusters not only in the ear skin but also in other regions, such as the back skin and the footpad (**Supplementary Fig. 3d**). These results suggested that the formation of DC clusters was not an ear-specific event but was a general mechanism during skin inflammation.

The abundance of DC clusters in response to the application of DNFB was not altered in mice that lack T cells and B cells (recombinase

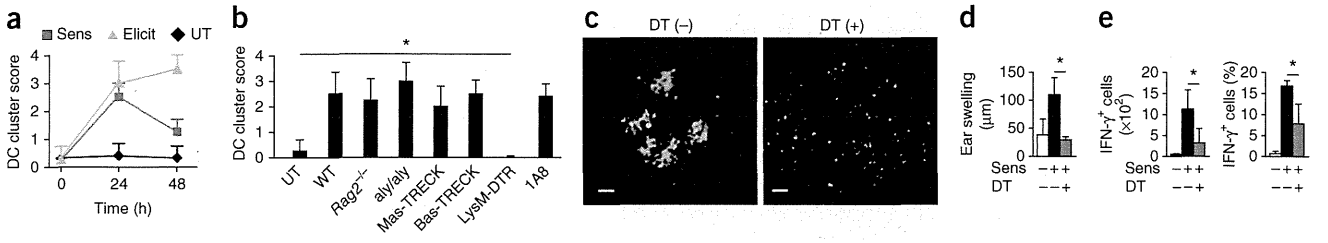

Figure 4 Macrophages are essential for DC cluster formation. (**a**) Score of DC cluster abundance in mice ($n = 4$ per group) left untreated (UT) or 24 h and 48 h after application of DNFB in the sensitization or elicitation phase of CHS; scores were assigned according to the size and number of clusters. (**b**) Score of DC cluster abundance (as in **a**) in untreated wild-type mice (UT), in DNFB-treated wild-type (C57BL/6) mice (WT), RAG-2-deficient mice (*Rag2*$^{-/-}$), aly/aly mice (aly/aly), DT-treated Mas-TRECK or Bas-TRECK mice or DT-treated C57BL/6 recipients of LysM-DTR BM cells, and in wild-type mice treated with 1A8 (anti-Ly6G) ($n = 4$ mice per group). (**c**) DC clusters in C57BL/6 chimeras given LysM-DTR BM with (right) or without (left) treatment of recipients with DT. Scale bars, 100 μm. (**d**) Ear swelling in C57BL/6 chimeras ($n = 5$ per group) given LysM-DTR BM with or without treatment with DT, assessed 24 h after no DNFB (Sense −) or application of DNFB to the recipients. (**e**) Quantification (left) and frequency (right) of IFN-γ-producing CD8$^+$ T cells in mice as in **d** ($n = 5$ per group). *$P < 0.05$ (unpaired Student's *t*-test). Data are representative of three (**a**,**c**,**e**), two (**b**) or four (**d**) experiments (error bars (**b**,**d**,**e**), s.d.).

RAG-2–deficient mice), in mice deficient in lymphoid tissue–inducer cells (alymphoblastic (aly/aly) mice)[12] or in mice depleted of mast cells or basophils (Mas-TRECK or Bas-TRECK mice treated with DT)[13,14] (**Fig. 4b**). In contrast, DC clustering was abrogated in C57BL/6 mice given transfer of BM from LysM-DTR mice (with sequence encoding a DTR cassette inserted into the gene encoding lysozyme M) followed by treatment of the recipients with DT to ensure depletion of both macrophages and neutrophils (**Fig. 4b**,**c**). Depletion of neutrophils alone, by administration of antibody 1A8 to Ly6G, did not interfere with the formation of DC clusters (**Fig. 4b**), which suggested that macrophages were required during the formation of DC clusters, but neutrophils were not. Of note, the formation of DC clusters was not attenuated by treatment with the LFA-1-neutralizing antibody KBA (**Supplementary Fig. 3e**,**f**), which suggested that macrophage-DC interactions were LFA-1 independent. Consistent with the formation of DC clusters, elicitation of the CHS response (**Fig. 4d**) and IFN-γ production by skin T cells (**Fig. 4e**) were significantly suppressed in chimeras given LysM-DTR BM and treated with DT. Thus, skin macrophages were required for the formation of DC clusters, which was necessary for T cell activation and the elicitation of CHS.

Perivascular DCs clustering requires macrophages

To examine the migratory kinetics of dermal macrophages and DCs *in vivo*, we visualized them by two-photon microscopy. *In vivo* labeling of blood vessels with dextran conjugated to the hydrophobic red fluorescent dye TRITC (tetramethylrhodamine isothiocyanate) revealed that dDCs distributed diffusely in the steady state (**Fig. 5a**, left). After application of DNFB to the ears of mice previously sensitized with DNFB, dDCs accumulated mainly around post-capillary venules (**Fig. 5a**, right, and **b**). Time-lapse imaging revealed that some dDCs showed directional migration toward TRITC$^+$ cells that were labeled red by incorporation of extravasated TRITC-dextran (**Fig. 5c** and **Supplementary Movie 4**). Most of the TRITC$^+$ cells were F4/80$^+$CD11b$^+$ macrophages (**Supplementary Fig. 4a**). These observations prompted us to investigate the role of macrophages in DC accumulation. We used a chemotaxis assay to determine whether macrophages attracted the DCs. We isolated dDCs and dermal macrophages from dermal skin cell suspensions and incubated them for 12 h in a Transwell assay. dDCs placed in the upper wells migrated efficiently to lower wells that contained dermal macrophages (**Fig. 5d**). However, we did not observe such dDC migration when macrophages were absent from the lower wells (**Fig. 5d**). Thus, dermal macrophages were able to attract dDCs *in vitro*, which may have led to the accumulation of dDCs around post-capillary venules.

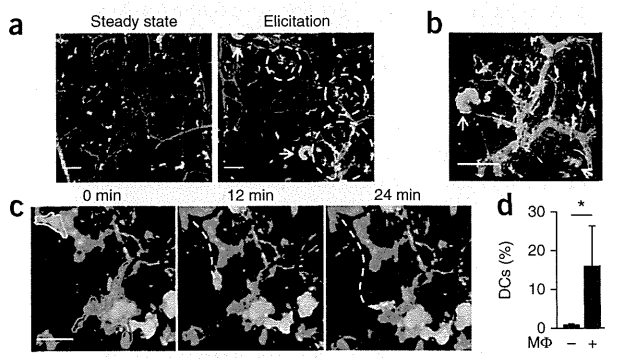

Figure 5 Macrophages mediate the perivascular formation of DC clusters. (**a**) Distribution of dDCs (green) in the steady state (left) and in the elicitation phase of CHS (right). White outlined areas indicate DC clusters; arrows indicate sebaceous glands visualized with BODIPY (green); yellow and red, blood vessels; red, macrophages. Scale bars, 100 μm. (**b**) Enlargement of a perivascular DC cluster. Arrows indicate sebaceous glands of hair follicles. Scale bar, 100 μm.(**c**) Sequential images of dDCs (green) and macrophages (red) in the elicitation phase of CHS. White dashed line represents the track of a DC. Scale bar, 30 μm. (**d**) Chemotaxis of dDCs in the presence (+) or absence (−) of macrophages (MΦ) prepared from ear skin, presented as the frequency of dDCs that transmigrated into the lower chamber of a Transwell (relative to input dDCs). *$P < 0.05$ (unpaired Student's *t*-test). Data are representative of three experiments (error bars (**d**), s.d.).

DC cluster formation requires IL-1α upon antigen challenge

We attempted to explore the mechanism underlying the formation of DC clusters. We observed that DC accumulation occurred during the first application of hapten (**Fig. 4a**), which suggested that an antigen-nonspecific mechanism, such as production of the proinflammatory mediator IL-1, may initiate DC clustering. DNFB-induced accumulation of DCs was not suppressed in mice deficient in NLRP3 or deficient in caspase-1 and caspase-11 more than their wild-type counterparts, but it was significantly lower in IL-1R1-deficient mice (which lack the receptor for IL-1α and IL-1β and for the IL-1 receptor antagonist (IL-1ra)) than in their wild-type counterparts, as well as after the subcutaneous administration of IL-1ra than before treatment with the antagonist (**Fig. 6a**,**b**). Consistent with those observations, the elicitation of CHS and IFN-γ production by skin T cells were significantly attenuated in mice that lacked both IL-1α and IL-1β (**Fig. 6c**,**d**). In addition, the formation of dDC clusters was suppressed significantly by the subcutaneous injection of a neutralizing antibody to IL-1α but

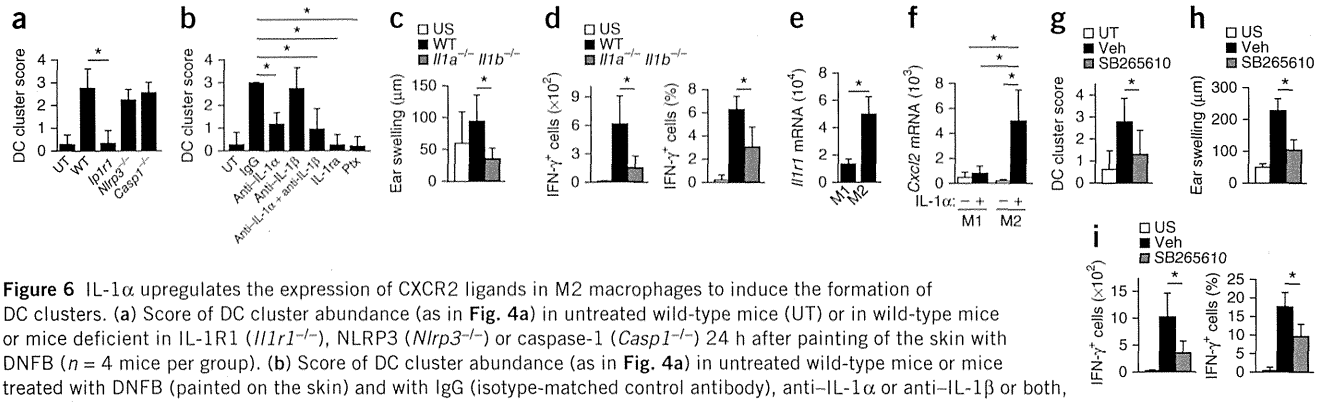

Figure 6 IL-1α upregulates the expression of CXCR2 ligands in M2 macrophages to induce the formation of DC clusters. (**a**) Score of DC cluster abundance (as in **Fig. 4a**) in untreated wild-type mice (UT) or in wild-type mice or mice deficient in IL-1R1 (*Il1r1*$^{-/-}$), NLRP3 (*Nlrp3*$^{-/-}$) or caspase-1 (*Casp1*$^{-/-}$) 24 h after painting of the skin with DNFB ($n = 4$ mice per group). (**b**) Score of DC cluster abundance (as in **Fig. 4a**) in untreated wild-type mice or mice treated with DNFB (painted on the skin) and with IgG (isotype-matched control antibody), anti–IL-1α or anti–IL-1β or both, recombinant IL-1ra or pertussis toxin (Ptx), assessed 24 h after treatment with hapten ($n = 4$ mice per group). (**c**,**d**) Ear swelling 24 h after application of DNFB (**c**) and quantification (**d**, left) and frequency (**d**, right) of IFN-γ-producing CD8$^+$ T cells in the ear 18 h after application of DNFB (**d**) in unsensitized wild-type mice (US) or in mice lacking both IL-1α and IL-1β (*Il1a*$^{-/-}$*Il1b*$^{-/-}$) and wild-type mice given adoptive transfer of DNFB-sensitized T cells ($n = 5$ mice per group). (**e**) Quantitative RT-PCR analysis of *Il1r1* mRNA in M1 or M2 macrophages ($n = 4$ mice per group). (**f**) Quantitative RT-PCR analysis of *Cxcl2* mRNA in M1 or M2 macrophages cultured with (+) or without (–) IL-1α. (**g**) Score of DC cluster abundance (as in **Fig. 4a**) in untreated wild-type mice (UT) or in mice treated with DNFB (painted on the skin) in the presence (SB265610) or absence (vehicle (Veh)) of a CXCR2 inhibitor, assessed 24 h after treatment with DNFB ($n = 4$ mice per group). (**h**,**i**) Ear swelling 24 h after application of DNFB (**h**) and quantification (**i**, right) and frequency (**i**, left) of IFN-γ-producing CD8$^+$ T cells 18 h after application of DNFB (**i**) in unsensitized wild-type mice (US) or in mice treated with DNFB in the presence or absence of the CXCR2 inhibitor SB265610 ($n = 5$ mice per group). $^*P < 0.05$ (unpaired Student's *t*-test). Data are representative of two (**a**,**c**,**d**) or three (**b**,**e**–**i**) experiments (error bars, s.d.).

was suppressed only marginally by a neutralizing antibody to IL-1β (**Fig. 6b**). Because keratinocytes are known to produce IL-1α upon application of a hapten[15], our results suggested a major role for IL-1α in mediating the formation of DC clustering.

M2 macrophages produce chemokine CXCL2 to attract dDCs

To further characterize how macrophages attract dDCs, we examined expression of the gene encoding IL-1Rα (*Il1r1*) in BM-derived classically activated (M1) and alternatively activated (M2) macrophages, classified as such on the basis of differences in the expression of *Tnf*, *Nos2*, *Il12a*, *Arg1*, *Retnla* and *Chi313* mRNA[16] (**Supplementary Fig. 4b**). We found that M2 macrophages had higher expression of *Il1r1* mRNA than did M1 macrophages (**Fig. 6e**). We also found that subcutaneous injection of pertussis toxin, an inhibitor specific for inhibitory regulative G protein, almost completely abrogated the formation of DC clusters in response to hapten stimuli (**Fig. 6b**), which suggested that signaling through chemokines coupled to the inhibitory regulative G protein was required for the formation of DC clusters.

We next used microarray analysis to examine the effect of IL-1α on the expression of chemokine-encoding genes in M1 and M2 macrophages. Treatment with IL-1α did not enhance such expression in M1 macrophages, whereas it increased the expression of *Ccl5*, *Ccl17*, *Ccl22* and *Cxcl2* mRNA in M2 macrophages (**Supplementary Table 1**). Among those, *Cxcl2* mRNA expression was enhanced most prominently by treatment with IL-1α, a result we confirmed by real-time PCR analysis (**Fig. 6f**). Consistently, *Cxcl2* mRNA expression was much higher in DNFB-painted skin than in untreated skin (**Supplementary Fig. 5a**) and was not affected by neutrophil depletion with the 1A8 antibody to Ly6G (**Supplementary Fig. 5b**,**c**). In addition, IL-1α-treated dermal macrophages produced *Cxcl2* mRNA *in vitro* (**Supplementary Fig. 5d**). These results suggested that dermal macrophages, but not neutrophils, were the main source of CXCL2 during CHS. We also detected high expression of *Cxcr2* mRNA (which encodes the receptor for CXCL2) in DCs (**Supplementary Fig. 5e**); this prompted us to examine the role of CXCR2 in dDCs. The formation of DC clusters in response to DNFB was substantially reduced by intraperitoneal administration of the CXCR2 inhibitor SB265610 (ref. 17) (**Fig. 6g**). In addition, treatment with SB265610 during the elicitation of CHS with DNFB inhibited ear swelling (**Fig. 6h**) and IFN-γ production by skin T cells (**Fig. 6i**).

Together our results indicated that in the absence of effector T cells specific for a cognate antigen (i.e., in the sensitization phase of CHS), DC clustering was a transient event, and hapten-carrying DCs migrated into draining LNs to establish sensitization. On the other hand, in the presence of the antigen and antigen-specific effector or memory T cells, DC clustering was followed by accumulation of T cells (i.e., in the elicitation phase of CHS) (**Supplementary Fig. 6**). Thus, dermal macrophages were essential for initiating the formation of DC clusters through the production of CXCL2, and DC clustering had a role in the efficient activation of skin T cells.

DISCUSSION

Although the mechanistic events in the sensitization phase in cutaneous immunity have been studied thoroughly over 20 years[18,19], the types of immunological events that occur during the elicitation phases in the skin has remained unclear. Here we have described the antigen-dependent induction of DC–T cell clusters in the skin in a mouse model of CHS and showed that DC–effector T cell interactions in these clusters were required for the induction of efficient antigen-specific immune responses in the skin. We found that dDCs, but not epidermal LCs, were essential for the presentation of antigen to skin effector T cells and that they exhibited sustained association with effector T cells in an antigen- and LFA-1-dependent manner. IL-1α, not the inflammasome, initiated the formation of these perivascular DC clusters.

Epidermal contact with antigens triggers the release of IL-1 in the skin[15]. Published studies have shown that the epidermal keratinocytes constitute a major reservoir of IL-1α[6] and that mechanical stress applied to keratinocytes permits the release of large amounts of IL-1α even in the absence of cell death[20]. The cellular source of IL-1α in this process remains unclear. We found that IL-1α activated macrophages that subsequently attracted dDCs, mainly to areas around post-capillary venules, where effector T cells are known to transmigrate from the blood into the skin[21]. In the presence of the antigen and antigen-specific

effector T cells, DC clustering was followed by T cell accumulation. Therefore, we propose that these perivascular dDC clusters may provide antigen-presentation sites for efficient activation of effector T cells. This is suggested by the observations that CHS responses and intracutaneous T cell activation were attenuated substantially in the absence of these clusters, in conditions of macrophage depletion or inhibition of integrin function, IL-1R signaling[22,23] or CXCR2 signaling[24].

In contrast to antigen presentation in the skin, antigen presentation in other peripheral barrier tissues is relatively well understood. In submucosal areas, specific sentinel lymphoid structures (mucosa-associated lymphoid tissue (MALT)) serve as peripheral antigen-presentation sites[25], and lymphoid follicles are present in non-inflammatory bronchi (bronchus-associated lymphoid tissue (BALT)). These structures serve as antigen-presentation sites in nonlymphoid peripheral organs. By analogy, the concept of skin-associated lymphoid tissue (SALT) was proposed in the early 1980s, on the basis of findings that cells in the skin are able to capture, process and present antigens[26,27]. However, the role of cellular skin components as antigen-presentation sites has remained uncertain. Here we have identified an inducible structure formed by dermal macrophages, dDCs and effector T cells, which seemed to accumulate sequentially. Because formation of this structure was essential for efficient activation of effector T cells, these inducible leukocyte clusters may function as SALTs. Unlike leukocyte clusters in MALT, these leukocyte clusters were not found in the steady state but were induced during the development of an adaptive immune response. Therefore, these clusters might be better called 'inducible SALTs', similar to inducible BALTs in the lung[28]. In contrast to the cells present in inducible BALT, we did not identify naive T cells or B cells in SALT (data not shown), which suggested that the leukocyte clusters in the skin may be specialized for the activation of effector T cells but not for the activation of naive T cells. Our findings suggest that approaches for the selective inhibition of this structure may have novel therapeutic benefit in inflammatory disorders of the skin.

METHODS

Methods and any associated references are available in the online version of the paper.

Accession codes. GEO: microarray data, GSE53680.

Note: Any Supplementary Information and Source Data files are available in the online version of the paper.

ACKNOWLEDGMENTS

We thank H. Yagita (Juntendo University) for the KBA neutralizing antibody to LFA-1; P. Bergstresser and J. Cyster for critical reading of our manuscript. Supported by grants-in-aid for Scientific Research from the Ministry of Education, Culture, Sports, Science and Technology of Japan.

AUTHOR CONTRIBUTIONS

Y.N., G.E. and K.K. designed this study and wrote the manuscript; Y.N., G.E., S. Nakamizo, S.O., S.H., N.K., A.O., A.K., T. Honda and S. Nakajima performed the experiments and analyzed data; S.T. and Y.S. did experiments related to microarray analysis; K.J.I., H.T., H.Y., Y.I., M.K. and L.g.N. developed experimental reagents and gene-targeted mice; J.F. and E.G.-Y. did experiments related to immunohistochemistry of human samples; T.O., T. Hashimoto, Y.M. and K.K. directed the project and edited the manuscript; and all authors reviewed and discussed the manuscript.

COMPETING FINANCIAL INTERESTS

The authors declare no competing financial interests.

1. von Andrian, U.H. & Mempel, T.R. Homing and cellular traffic in lymph nodes. *Nat. Rev. Immunol.* **3**, 867–878 (2003).
2. Clark, R.A. *et al.* The vast majority of CLA+ T cells are resident in normal skin. *J. Immunol.* **176**, 4431–4439 (2006).
3. Wang, L. *et al.* Langerin expressing cells promote skin immune responses under defined conditions. *J. Immunol.* **180**, 4722–4727 (2008).
4. Tuckermann, J.P. *et al.* Macrophages and neutrophils are the targets for immune suppression by glucocorticoids in contact allergy. *J. Clin. Invest.* **117**, 1381–1390 (2007).
5. Sims, J.E. & Smith, D.E. The IL-1 family: regulators of immunity. *Nat. Rev. Immunol.* **10**, 89–102 (2010).
6. Murphy, J.E., Robert, C. & Kupper, T.S. Interleukin-1 and cutaneous inflammation: a crucial link between innate and acquired immunity. *J. Invest. Dermatol.* **114**, 602–608 (2000).
7. Nakae, S. *et al.* IL-1-induced tumor necrosis factor-α elicits inflammatory cell infiltration in the skin by inducing IFN-γ-inducible protein 10 in the elicitation phase of the contact hypersensitivity response. *Int. Immunol.* **15**, 251–260 (2003).
8. Thyssen, J.P., Linneberg, A., Menne, T., Nielsen, N.H. & Johansen, J.D. Contact allergy to allergens of the TRUE-test (panels 1 and 2) has decreased modestly in the general population. *Br. J. Dermatol.* **161**, 1124–1129 (2009).
9. Ng, L.G. *et al.* Migratory dermal dendritic cells act as rapid sensors of protozoan parasites. *Plos Pathog* **4**, e1000222 (2008).
10. Springer, T.A. & Dustin, M.L. Integrin inside-out signaling and the immunological synapse. *Curr. Opin. Cell Biol.* **24**, 107–115 (2012).
11. Egawa, G. *et al. In vivo* imaging of T-cell motility in the elicitation phase of contact hypersensitivity using two-photon microscopy. *J. Invest. Dermatol.* **131**, 977–979 (2011).
12. Miyawaki, S. *et al.* A new mutation, aly, that induces a generalized lack of lymph nodes accompanied by immunodeficiency in mice. *Eur. J. Immunol.* **24**, 429–434 (1994).
13. Sawaguchi, M. *et al.* Role of mast cells and basophils in IgE responses and in allergic airway hyperresponsiveness. *J. Immunol.* **188**, 1809–1818 (2012).
14. Otsuka, A. *et al.* Requirement of interaction between mast cells and skin dendritic cells to establish contact hypersensitivity. *PLoS ONE* **6**, e25538 (2011).
15. Enk, A.H. & Katz, S.I. Early molecular events in the induction phase of contact sensitivity. *Proc. Natl. Acad. Sci. USA* **89**, 1398–1402 (1992).
16. Weisser, S.B., McLarren, K.W., Kuroda, E. & Sly, L.M. Generation and characterization of murine alternatively activated macrophages. *Methods Mol. Biol.* **946**, 225–239 (2013).
17. Liao, L. *et al.* CXCR2 blockade reduces radical formation in hyperoxia-exposed newborn rat lung. *Pediatr. Res.* **60**, 299–303 (2006).
18. Honda, T., Egawa, G., Grabbe, S. & Kabashima, K. Update of immune events in the murine contact hypersensitivity model: toward the understanding of allergic contact dermatitis. *J. Invest. Dermatol.* **133**, 303–315 (2013).
19. Kaplan, D.H., Igyarto, B.Z. & Gaspari, A.A. Early immune events in the induction of allergic contact dermatitis. *Nat. Rev. Immunol.* **12**, 114–124 (2012).
20. Lee, R.T. *et al.* Mechanical deformation promotes secretion of IL-1 alpha and IL-1 receptor antagonist. *J. Immunol.* **159**, 5084–5088 (1997).
21. Sackstein, R., Falanga, V., Streilein, J.W. & Chin, Y.H. Lymphocyte adhesion to psoriatic dermal endothelium is mediated by a tissue-specific receptor/ligand interaction. *J. Invest. Dermatol.* **91**, 423–428 (1988).
22. Kish, D.D., Gorbachev, A.V. & Fairchild, R.L. IL-1 receptor signaling is required at multiple stages of sensitization and elicitation of the contact hypersensitivity response. *J. Immunol.* **188**, 1761–1771 (2012).
23. Kondo, S. *et al.* Interleukin-1 receptor antagonist suppresses contact hypersensitivity. *J. Invest. Dermatol.* **105**, 334–338 (1995).
24. Cattani, F. *et al.* The role of CXCR2 activity in the contact hypersensitivity response in mice. *Eur. Cytokine Netw.* **17**, 42–48 (2006).
25. Brandtzaeg, P., Kiyono, H., Pabst, R. & Russell, M.W. Terminology: nomenclature of mucosa-associated lymphoid tissue. *Mucosal Immunol.* **1**, 31–37 (2008).
26. Streilein, J.W. Skin-associated lymphoid tissues (SALT): origins and functions. *J. Invest. Dermatol.* **80** (suppl.), 12s–16s (1983).
27. Egawa, G. & Kabashima, K. Skin as a peripheral lymphoid organ: revisiting the concept of skin-associated lymphoid tissues. *J. Invest. Dermatol.* **131**, 2178–2185 (2011).
28. Moyron-Quiroz, J.E. *et al.* Role of inducible bronchus associated lymphoid tissue (iBALT) in respiratory immunity. *Nat. Med.* **10**, 927–934 (2004).

ONLINE METHODS

Mice. 8- to 12-week-old female C57BL/6 mice were used in this study. C57BL/6N mice were from SLC. Langerin-eGFP-DTR mice[29], CD11c-DTR mice[30], CD11c-YFP mice (that express CD11c tagged with YFP)[31], LysM-DTR mice[32], RAG-2-deficient mice[33], Mas-TRECK mice[13,14], Bas-TRECK mice[13,14], ALY/NscJcl- aly/aly mice[12], IL-1α/β-deficient mice[34], IL-1R1-deficient mice[35], NLRP3-deficient mice[36] and caspase-1/11-deficient mice[37] have been described. All experimental procedures were approved by the Institutional Animal Care and Use Committee of Kyoto University Graduate School of Medicine.

Human subjects. Biopsy samples of human skin were obtained from a nickel-reactive patch after 48 h after placement of nickel patch tests in patients with previously proven allergic contact dermatitis. A biopsy of petrolatum-occluded skin was also obtained as a control. Informed consent was obtained under protocols approved by the Institutional Review Board at the Icahn School of Medicine at Mount Sinai School Medical Center, and the Rockefeller University in New York.

Induction of CHS responses. Mice were sensitized on shaved abdominal skin with 25 μl 0.5% (wt/vol) DNFB (1-fluoro-2,4-dinitrofluorobenzene ; Nacalai Tesque) dissolved in acetone and olive oil (at a ratio of 4:1). Five days later, the ears were challenged with 20 μl 0.3% DNFB. For adoptive transfer, T cells were magnetically sorted, with an autoMACS (Miltenyi Biotec), from the draining LNs of sensitized mice and then were transferred intravenously (1×10^7 cells) into naive mice.

Depletion of cutaneous DC subsets, macrophages and neutrophils. For depletion of all cutaneous DC subsets (including LCs), 6-week-old Langerin-DTR mice were irradiated (two doses of 550 rads given 3 h apart) and were given transfer of 1×10^7 BM cells from CD11c-DTR mice. Eight weeks later, 2 μg DT (Sigma-Aldrich) was injected intraperitoneally. For selective depletion of LCs, irradiated Langerin-DTR mice were given transfer of BM cells from C57BL/6 mice, and 1 μg DT was injected. For selective depletion of dDCs, irradiated C57BL/6 mice were given transfer of BM cells from CD11c-DTR mice, and 2 μg DT was injected. For depletion of macrophages, irradiated C57BL/6 mice were given transfer of BM cells from LysM-DTR mice and 800 ng DT was injected. For depletion of neutrophils, anti-Ly6G (1A8; BioXCell) was administered to mice intravenously at a dose of 0.5 mg per mouse 24 h before experiments.

Time-lapse imaging of cutaneous DCs, macrophages and T cells. Cutaneous DCs were observed in CD11c-YFP mice. For labeling of cutaneous macrophages *in vivo*, 5 mg TRITC-dextran (Sigma-Aldrich) was injected intravenously and mice were allowed to 'rest' for 24 h. At that time, cutaneous macrophages became fluorescent because they had incorporated extravasated dextran. For labeling of skin-infiltrating T cells, T cells from DNFB-sensitized mice were labeled with CellTracker Orange (CMTMR (5-(and-6)-(((4-chloromethyl)benzoyl) amino)tetramethylrhodamine); Invitrogen) and were adoptively transferred into recipient mice. Keratinocytes and sebaceous glands were visualized by subcutaneous injection of isolectin B4 (Invitrogen) and BODIPY (Molecular Probes), respectively. Mice were positioned on a heating plate on the stage of a two-photon IX-81 microscope (Olympus) and their ear lobes were fixed beneath a cover slip with a single drop of immersion oil. Stacks of ten images, spaced 3 μm apart, were acquired at intervals of 1–7 min for up to 24 h. For calculation of T cell and DC velocities, movies were processed and analyzed with Imaris 7.2.1 software (Bitplane).

Histology and immunohistochemistry. For histological examination, tissues were fixed with 10% formalin in phosphate-buffered saline, then were embedded in paraffin. Sections with a thickness of 5 μm were prepared and then were stained with hematoxylin and eosin. For whole-mount staining, the ears were split into dorsal and ventral halves and were incubated for 30 min at 37 °C with 0.5 M ammonium thiocyanate. Then the dermal sheets were separated and fixed in acetone for 10 min at −20 °C. After treatment with Image-iT FX Signal Enhancer (Invitrogen), the sheets were incubated with antibody to mouse MHC class II (M5/114.15.2; eBioscience) followed by incubation with antibody to rat IgG conjugated to Alexa Fluor 488 (A-11006; Invitrogen) or Alexa Fluor 594 (A-11007; Invitrogen). The slides were mounted with a ProLong Antifade kit with the DNA-binding dye DAPI (4′6-diamidino-2-phenylindole; Molecular Probes) and were observed with a fluorescent microscope (BZ-900; KEYENCE). The number and size of DC clusters were evaluated in ten fields of 1 mm^2 per ear and were assigned scores according to the criteria in **Supplementary Figure 5a**.

Cell isolation and flow cytometry. For the isolation of skin lymphocytes, the split ears were incubated for 1 h at 37 °C in digestion buffer (RPMI medium supplemented with 2% FCS, 0.33 mg/ml of Liberase TL (Roche) and 0.05% DNase I (Sigma-Aldrich)). After that incubation, the tissues were disrupted by passage through a 70-μm cell strainer and stained with the appropriate antibodies (identified below). For analysis of intracellular cytokine production, cell suspensions were obtained in the presence of 10 μg/ml of brefeldin A (Sigma-Aldrich) and were fixed with Cytofix Buffer and permeabilized with Perm/Wash Buffer according to the manufacturer's protocol (BD Biosciences). Cells were stained with the following: antibody to mouse CD4 (GK1.5), anti-CD8 (53-6.7), anti-CD11b (M1/70), anti-CD11c (N418), anti-B220 (RA3-6B2), antibody to MHC class II (M5/114.15.2), anti-F4/80 (BM8), anti-IFN-γ (XMG1.2), anti-Gr1 (RB6-8c5) and 7-amino-actinomycin D (all from eBioscience); anti-mouse CD45 (30-F11) and anti-TCR-β (H57-597; both from BioLegend); and anti-CD16-CD32 (2.4G2; BD Biosciences). Flow cytometry was done with an LSR Fortessa (BD Biosciences) and data were analyzed with FlowJo software (TreeStarA).

Chemotaxis assays. Chemotaxis was assessed as described with some modifications[38]. The dermis of the ear skin was minced and then was digested for 30 min at 37 °C with 2 mg/ml collagenase type II (Worthington Biochemical) containing 1 mg/ml hyaluronidase (Sigma-Aldrich) and 100 μg/ml DNase I (Sigma-Aldrich). DDCs and macrophages were isolated with an autoMACS. Alternatively, BM-derived DCs and macrophages were prepared. 1×10^6 DCs were added to a Transwell insert with a pore size of 5 μm (Corning), and 5×10^5 macrophages were added to the lower wells, and the cells were incubated for 12 h at 37 °C. A known number of fluorescent reference beads (FlowCount fluorospheres; Beckman Coulter) were added to each sample to allow accurate quantification of cells that had migrated to the lower wells by flow cytometry.

Cell proliferation assay. Mice were sensitized with 25 μl 0.5% DNFB or 7% trinitrochlorobenzene (Chemical Industry). Five days later, T cells were magnetically separated from the draining LNs of each group of mice and were labeled with CellTrace Violet according to the manufacturer's protocol (Invitrogen). 1×10^6 T cells were adoptively transferred into naive mice, and the ears of the recipient mice were challenged with 20 μl of 0.5% DNFB. 24 h later, ears were collected and analyzed by flow cytometry.

***In vitro* differentiation of DCs and M1 and M2 macrophages from BM cells.** BM cells from the tibias and fibulas were plated at a density of 5×10^6 cells per 10-cm dish on day 0. For DC differentiation, cells were cultured at 37 °C in 5% CO_2 in cRPMI medium (RPMI medium supplemented with 1% L-glutamine, 1% HEPES, 0.1% 2-mercaptoethanol and 10% FBS) containing 10 ng/ml granulocyte-macrophage colony-stimulating factor (Peprotech). For macrophage differentiation, BM cells were cultured in cRPMI medium containing 10 ng/ml macrophage colony-stimulating factor (Peprotech). The medium was replaced on days 3 and 6 and cells were harvested on day 9. For the induction of M1 macrophages or M2 macrophages, cells were stimulated for 48 h with IFN-γ (10 ng/ml; R&D Systems) or with IL-4 (20 ng/ml; R&D Systems), respectively.

***In vitro* IL-1α-stimulation assay of dermal macrophages.** Dermal macrophages were separated from mice deficient in IL-1α and IL-1β[34] to avoid preactivation during cell preparations. Split ears were treated for 30 min at 37 °C with 0.25% trypsin and EDTA for removal of the epidermis, then were minced and then incubated with collagenase as described above. $CD11b^+$ cells were separated by magnetic-activated cell sorting, and 2×10^5 cells per well in 96-well plates were incubated for 24 h with or without 10 ng/ml IL-1α (R&D Systems).

doi:10.1038/ni.2992

Blocking assay. For the LFA-1-blocking assay, mice were given intravenous injection of 100 μg KBA (neutralizing antibody to LFA-1; a gift from H. Yagita) 12–14 h after challenge with 20 μl 0.5% DNFB. For blockade of IL-1R, mice were given subcutaneous injection of 10 μg recombinant mouse IL-1ra (PROSPEC) 5 h before challenge. For blockade of CXCR2, mice were given intraperitoneal treatment with 50 μg CXCR2 inhibitor[17] (SB265610; Tocris Bioscience) 6 h before and at the time of painting of the skin with hapten.

Quantitative PCR analysis. Total RNA was isolated with an RNeasy Mini kit (Qiagen, Hilden, Germany). cDNA was synthesized with a PrimeScript RT reagent kit and random hexamers according to the manufacturer's protocol (TaKaRa). A LightCycler 480 and LightCycler SYBR Green I Master mix were used according to the manufacturer's protocol (Roche) for quantitative PCR (primer sequences, **Supplementary Table 2**). The expression of each gene was normalized to that of the control gene *Gapdh*.

Microarray analysis. Total RNA was isolated with an RNeasy Mini Kit according to the manufacturer's protocol (Qiagen). An amplified sense-strand DNA product was synthesized with the Ambion WT Expression Kit (Life Technologies), was fragmented and labeled by the WT Terminal Labeling and Controls Kit (Affymetrix) and was hybridized to a Mouse Gene 1.0 ST Array (Affymetrix). We used the robust multiarray average algorithm for log transformation ($\log_2$) and normalization of the GeneChip data.

General experimental design and statistical analysis. For animal experiments, a sample size of three to five mice per group was used on the basis of past experience in generating statistical significance. Mice were randomly assigned to study groups and no specific randomization or blinding protocol was used. Sample or mouse identity was not masked for any of these studies. Prism software (GraphPad) was used for statistical analyses. Normal distribution was assumed a priori for all samples. Unless indicated otherwise, an unpaired parametric *t*-test was used for comparison of data sets. In cases in which the data-point distribution was not Gaussian, a nonparametric *t*-test was also applied. *P* values of less than 0.05 were considered significant.

29. Kissenpfennig, A. *et al.* Dynamics and function of Langerhans cells *in vivo*: dermal dendritic cells colonize lymph node areas distinct from slower migrating Langerhans cells. *Immunity* **22**, 643–654 (2005).
30. Jung, S. *et al. In vivo* depletion of CD11c$^+$ dendritic cells abrogates priming of CD8$^+$ T cells by exogenous cell-associated antigens. *Immunity* **17**, 211–220 (2002).
31. Lindquist, R.L. *et al.* Visualizing dendritic cell networks *in vivo*. *Nat. Immunol.* **5**, 1243–1250 (2004).
32. Miyake, Y. *et al.* Protective role of macrophages in noninflammatory lung injury caused by selective ablation of alveolar epithelial type II Cells. *J. Immunol.* **178**, 5001–5009 (2007).
33. Hao, Z. & Rajewsky, K. Homeostasis of peripheral B cells in the absence of B cell influx from the bone marrow. *J. Exp. Med.* **194**, 1151–1164 (2001).
34. Horai, R. *et al.* Production of mice deficient in genes for interleukin (IL)-1α, IL-1β, IL-1α/β, and IL-1 receptor antagonist shows that IL-1β is crucial in turpentine-induced fever development and glucocorticoid secretion. *J. Exp. Med.* **187**, 1463–1475 (1998).
35. Coban, C. *et al.* Immunogenicity of whole-parasite vaccines against *Plasmodium falciparum* involves malarial hemozoin and host TLR9. *Cell Host Microbe* **7**, 50–61 (2010).
36. Martinon, F., Petrilli, V., Mayor, A., Tardivel, A. & Tschopp, J. Gout-associated uric acid crystals activate the NALP3 inflammasome. *Nature* **440**, 237–241 (2006).
37. Koedel, U. *et al.* Role of caspase-1 in experimental pneumococcal meningitis: evidence from pharmacologic caspase inhibition and caspase-1-deficient mice. *Ann. Neurol.* **51**, 319–329 (2002).
38. Tomura, M. *et al.* Activated regulatory T cells are the major T cell type emigrating from the skin during a cutaneous immune response in mice. *J. Clin. Invest.* **120**, 883–893 (2010).

Vaccine 32 (2014) 5607–5613

Contents lists available at ScienceDirect

Vaccine

journal homepage: www.elsevier.com/locate/vaccine

Protective properties of a fusion pneumococcal surface protein A (PspA) vaccine against pneumococcal challenge by five different PspA clades in mice

Zhenyu Piao[a,b], Yukihiro Akeda[a], Dan Takeuchi[a], Ken J. Ishii[c,d], Kimiko Ubukata[e], David E. Briles[g], Kazunori Tomono[b], Kazunori Oishi[f,*]

[a] Laboratory for Clinical Research on Infectious Disease, International Research Center for Infectious Diseases, Research Institute for Microbial Diseases, Osaka University, Japan
[b] Division of Infection Control and Prevention, Osaka University Graduate School of Medicine, Japan
[c] National Institute of Biomedical Innovation, Japan
[d] Laboratory of Vaccine Science, WPI Immunology Frontier Research Center, Osaka University, Japan
[e] Department of Infectious Diseases, Keio University School of Medicine, Japan
[f] Infectious Disease Surveillance Center, National Institute of Infectious Diseases, Japan
[g] Department of Microbiology, University of Alabama at Birmingham, USA

ARTICLE INFO

Article history:
Received 12 May 2014
Received in revised form 21 July 2014
Accepted 31 July 2014
Available online 12 August 2014

Keywords:
Streptococcus pneumoniae
PspA fusion protein
PspA vaccine
Cross-protection
Binding of PspA-specific IgG

ABSTRACT

An increase in the appearance of nonvaccine serotypes in both children and adults with invasive pneumococcal disease (IPD) after introduction of pneumococcal conjugate vaccine represents a limitation of this vaccine. In this study, we generated three recombinant pneumococcal surface protein A (PspA) proteins comprising PspA families 1 and 2, and we examined the reactivity of antisera raised in mice immunized with a PspA fusion protein in combination with CpG oligonucleotides plus aluminum hydroxide gel. The protective effects of immunization with PspA fusion proteins against pneumococcal challenge by strains with five different PspA clades were also examined in mice. Flow cytometry demonstrated that PspA3+2-induced antiserum showed the greatest binding of PspA-specific IgG to all five challenge strains with different clades. PspA2+4- or PspA2+5-induced antiserum showed the lowest binding of PspA-specific IgG to clade 3. Immunization with PspA3+2 afforded significant protection against pneumococcal challenge by five strains with different clades in mice, but immunization with PspA2+4 or PspA2+5 failed to protect mice from pneumococcal challenge by strains with clades 1 and 3. The binding of PspA-specific IgG in antisera raised by three PspA fusion proteins was examined in 68 clinical isolates from adult patients with IPD. Immunization of mice with PspA3+2-induced antiserum with a high binding capacity for clinical isolates expressing clades 1–4, but not clade 5. Our results suggest that the PspA3+2 vaccine has an advantage over the PspA2+4 or PspA2+5 vaccine in terms of a broad range of cross-reactivity with clinical isolates and cross-protection against pneumococcal challenge in mice.

1. Introduction

Streptococcus pneumoniae is a major cause of morbidity and mortality caused by pneumonia, bacteremia, and meningitis worldwide [1]. After introduction of the seven-valent pneumococcal conjugate vaccine (PCV7) in children, significant declines in the incidence of invasive pneumococcal disease (IPD) caused by vaccine serotypes were reported in children and adults [2,3]. However, an increase in the incidence of IPD caused by non-PCV7 serotypes has been also observed in children and adults [3–5]. In addition, after introduction of a 13-valent pneumococcal conjugate vaccine (PCV13) in children, serotypes not included in PCV13 have been isolated with increasing frequency in pediatric and adult patients with IPD [6,7]. Because there are >90 different pneumococcal capsular serotypes, continuous supplementation of pneumococcal conjugate vaccines with new serotypes for serotype replacement may not be a practical strategy.

Previous studies have demonstrated that several pneumococcal proteins are potential vaccine candidates [8–11]. One candidate protein antigen is pneumococcal surface protein A (PspA), which is

* Corresponding author. Tel.: +81 3 5285 1111; fax: +81 3 5285 1129.
E-mail address: oishik@nih.go.jp (K. Oishi).

http://dx.doi.org/10.1016/j.vaccine.2014.07.108
0264-410X/

an exposed virulence factor found in virtually all pneumococcal strains [12,13]. Anti-PspA antibodies overcome the anticomplement effect of PspA, allowing for increased complement activation and C3 deposition on PspA-bearing bacteria [14,15]. Serum from humans immunized with PspA can passively protect mice against challenge with various pneumococcal strains [16]. Importantly, a recent study confirmed that the rabbit antibodies to PspA could mediate killing in the modified opsonophagocytosis killing assay [17].

PspA is composed of five domains: (i) a signal peptide, (ii) an α-helical highly charged (N-terminal) domain, (iii) a proline-rich region domain, (iv) a choline-binding domain, and (v) a short hydrophobic tail [18,19]. The α-helical domain of PspA has an antiparallel coiled-coil motif and is considered to be the most exposed part of the molecule [20]. The α-helical domain binds to protective monoclonal antibodies and inhibits killing of pneumococci by at least two host cationic peptides [21,22]. The proline-rich domain is composed of many repetitive sequences shared by other proline-rich domains making its inclusion important for achieving broad protection [23].

PspA proteins have been grouped into three families encompassing six different clades based on the C-terminal 100 amino acids of the α-helical region [24]. Family 1 comprises clades 1 and 2; family 2 comprises clades 3, 4 and 5; and family 3 comprises clade 6 [22,24]. Pneumococcal strains expressing family 1 or 2 PspA proteins constitute >96% of clinical isolates from patients with IPD [6,13,25]. Although different PspA proteins induce antibodies with different degrees of cross-reactivity in vitro and cross-protection of mice [26,27], our previous studies demonstrated that no single PspA construct can elicit complete protection against challenge by strains with all PspA clades and families [28]. To accommodate this variability, it was proposed that a combination of two PspA antigens, one from PspA family 1 and one from PspA family 2, should elicit protection against the vast majority of pneumococcal strains [29–31]. Thus, it is important to determine which PspA fragments show the broadest cross-reactivity. In this study, we prepared fusion proteins of three pairs of PspA molecules, and determined which provided the broadest cross-reaction with clinical isolates of *S. pneumoniae*.

2. Materials and methods

2.1. Pneumococcal strains

Six laboratory strains (all originally from patients), including BG9739 (serotype 4, PspA clade 1), D39 (serotype 2, PspA clade 2), WU2 (serotype 3, PspA clade 2), TIGR4 (serotype 3, PspA clade 3), EF5668 (serotype 4, PspA clade 4), and ATCC 6303 (serotype 3, PspA clade 5) were used to construct the fusion PspA proteins. These laboratory strains and a recent clinical isolate, KK1162 (serotype 3, PspA clade 4), were used for bacterial challenge. Sixty-eight clinical isolates, including KK1162 strain, from Japanese adult patients with IPD were also used [32]. These isolates were serotyped using agglutination assay, and their PspA clades were determined using a method published previously [32,33].

2.2. Construction of fusion PspA fragments

Our previous study demonstrated a significant protection against sepsis caused by WU2 strain (PspA clade 1) by immunization with full-length BG9739 derived PspA (clade 1) but only a weak protection against homologous challenge with BG9739 [28]. Therefore, we excluded PspA clade 1 derived from BG9739 strain from the fusion PspA proteins. In this study, we prepared the fusion proteins from three pairs of PspA clade 2 from family 1 and PspA clades 3, 4 and 5 from family 2. All cloning procedures were performed with *Escherichia coli* DH5α grown in Luria–Bertani medium (Sigma-Aldrich, St. Louis, MO) supplemented with kanamycin (30 μg/ml). DNA fragments encoding portions of the N-terminal regions (containing the α-helix domain and proline-rich region) of PspA clades 2 and 3 were amplified by PCR using strains D39 and TIGR4. The primers used in this procedure are available in Appendix 1. The resulting PCR products were digested with *Nde*I and *Eco*RI, and were ligated to the pET28a (+) vector (Novagen, Madison, WI), and the sequences were confirmed by DNA sequencing. The pET28a–PspA constructs digested with *Eco*RI and *Xho*I, and the resulting fragments, which encoded portions of the N-terminal regions of PspA clades 4, 5, or 2 were amplified by PCR using strains EF5668 (Accession no. U89711), ATCC6303 (Accession no. AF071820), or WU2 (Accession no. AF071814), respectively, and were ligated to the linearized vector. The fusion PspA proteins were obtained with primers that allowed the removal of the signal sequence. The fusion PspA2+4 was constructed by fusing the 3′ terminus of PspA clade 2 of D39 strain (Accession no. AF071814) with the 5′ terminus of PspA clade 4 of EF5668 strain, through the *Eco*RI ligated to pET28a–6 × His. The fusion PspA2+5 was constructed by fusing the 3′ terminus of PspA clade 2 of D39 strain with the 5′ terminus of PspA clade 5 of ATCC6303 strain, through the *Eco*RI ligated to pET28a–6 × His. The fusion PspA3+2 was constructed by fusing the 3′ terminus of PspA clade 3 of TIGR4 strain (Accession no. AE005672.3) with the 5′ terminus of PspA clade 2 of WU2 strain, through the *Eco*RI ligated to pET28a–6 × His.

2.3. PspA expression and purification

Competent *E. coli* BL21 (DE3) cells were transformed with pET28a (+) vectors containing the fusion PspA or the single PspA constructs. The recombinant proteins were purified and stored as described elsewhere [34].

2.4. Immunization of mice

Female C57/BL6j mice (6–8 weeks old) were purchased from CLA Japan. Mice were immunized subcutaneously three times at 7-days intervals with 0.1 μg of recombinant fusion PspA derivatives in lipopolysaccharide-free phosphate-buffered saline (PBS) (Sigma) in combination with 2.5 μg of TLR9 ligand adjuvants K3 CpG oligonucleotides (CpG ODNs) and 5 μg of aluminum hydroxide gel (AHG) (A gift from The Research Foundation for Microbial Diseases of Osaka University) or CpG ODNs alone (final volume of 200 μl per mouse). A subcutaneous route of immunization was chosen because our preliminary study demonstrated the levels of PspA-specific IgG in mice subcutaneously immunized with 0.1 μg of PspA plus 2.5 μg of CpG ODNs were significantly higher than those in mice nasally immunized with 0.1 μg of PspA plus 2.5 μg of CpG ODNs (data not shown). CpG ODNs were prepared as described previously [35]. Because the PspA clade-specific IgG levels tended to be higher in mice immunized with each PspA fusion protein with CpG ODNs plus AHG than in those immunized with PspA fusion protein with CpG ODNs alone (see Appendix 2), we used the CpG ODNs plus AHG (define as the double adjuvants), for the immunization of mice with PspA fusion proteins in this study. These double adjuvants were safe in nonhuman primate models, and were applicable to humans [36]. Serum was collected from mice by retro-orbital bleeding 1 week after the third immunization. All animal experiments were approved by the Animal Care and Use Committee of the Research Institute for Microbial Diseases, Osaka University, Japan (Permit Number: Biken-AP-H23-05-0).

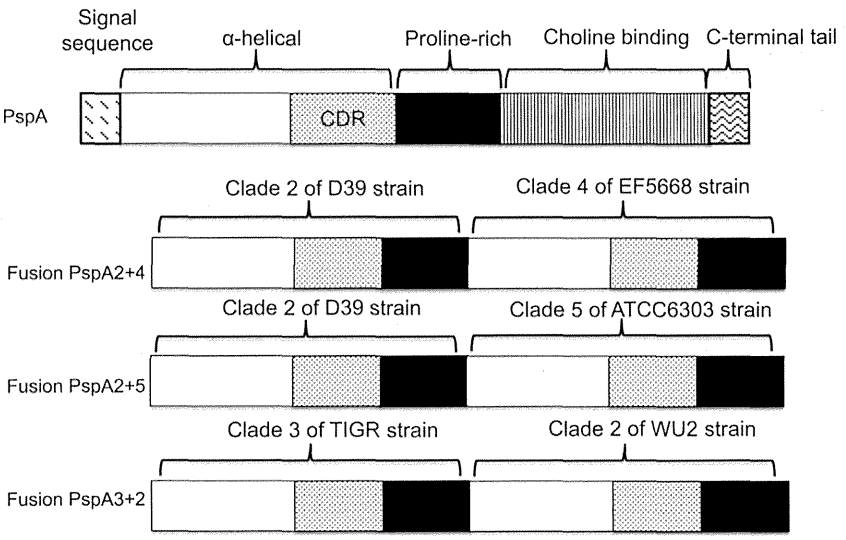

Fig. 1. Schematic diagram of PspA and three fusion PspA proteins. The entire PspA molecule containing the N-terminal α-helical domain, which contains the clade-defining region (CDR), the proline-rich region, the choline-binding domain, and the C-terminal tail (upper column). Each recombinant fusion protein is shown with its different composition (three lower rows).

2.5. Binding of PspA-specific IgG to pneumococcal strains by flow cytometry

Five pneumococcal strains for bacterial challenge and 68 clinical isolates were grown in blood agar plates overnight and then subcultured again on blood agar plates for 4–5 h. The bacteria were collected in PBS, harvested by centrifugation, and washed once with PBS. Ninety microliters of the bacterial suspension at a concentration of 1×10^8 colony-forming units (cfu)/ml in PBS was incubated with 10 μl of mouse antisera for 30 min at 37 °C. After incubation, the suspension was washed once with PBS, resuspended in 100 μl of fluorescein isothiocyanate-conjugated goat anti-mouse IgG (1:100), and incubated for 30 min on ice. After the incubation, the bacterial suspension was washed twice with PBS and suspended in 500 μl of 1% formaldehyde. The samples were kept on ice in the dark until analyzed by flow cytometry using a BD FACSCalibur™ with CellQuest software (BD Sciences, San Jose, CA), and the percentage of fluorescent bacteria (>1 fluorescence intensity unit) in each group was determined. Sera from mice immunized with double adjuvants only were used as the negative controls.

2.6. Protection against pneumococcal challenge

The mice immunized with the PspA fusion protein plus double adjuvants were challenged intranasally with 2×10^7 cfu of strain BG9739 (clade 1), 2×10^7 cfu of strain WU2 (clade 2), 5×10^6 cfu of strain TIGR4, 2×10^7 cfu of strain KK1162 (clade 4), or 5×10^5 cfu of strain ATCC6303 (clade 5). Bacterial challenges were performed 2 weeks after the final immunization. Mortality was monitored for 2 weeks following pneumococcal challenge. The mice immunized with double adjuvants alone were used as a control.

2.7. Statistical analysis

Analysis of variance followed by an unpaired Mann–Whitney *U* test was used to evaluate differences in antibody titer. The percent binding by immune sera to each pneumococcal strain was compared by paired *t*-test. Survival rates were analyzed by the Kaplan–Meier log-rank test. All analyses were performed using GraphPad Prism Software (GraphPad software, La Jolla, CA). *p* values <0.05 were considered significant.

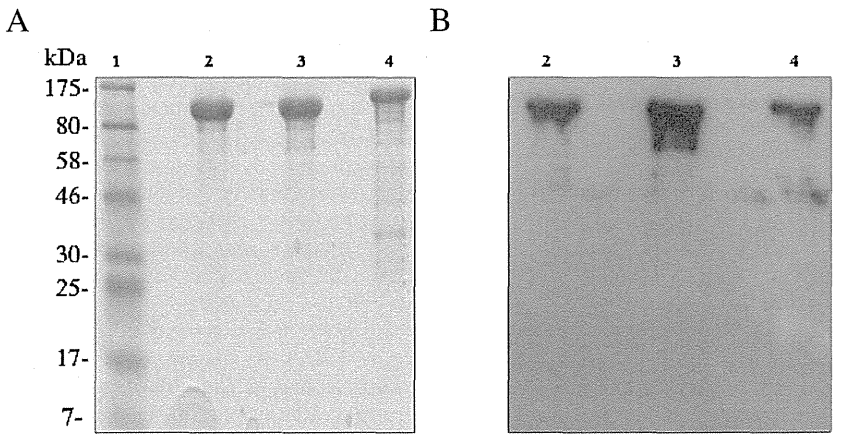

Fig. 2. Characterization of three purified fusion PspA proteins by SDS–PAGE (A) and Western blot analysis (B). The proteins were subjected to SDS–PAGE and detected by direct staining with Coomassie brilliant blue. Lane 1, standard molecular weight markers; lane 2, PspA2+4; lane 3, PspA2+5; 4, lane PspA3+2. The values on the left are molecular sizes in kilodaltons. Mouse antiserum against PspA recombinant protein (clade 2) was used for Western blot analysis. Lane 2, PspA2+4; lane 3, PspA2+5; lane 4, PspA3+2.

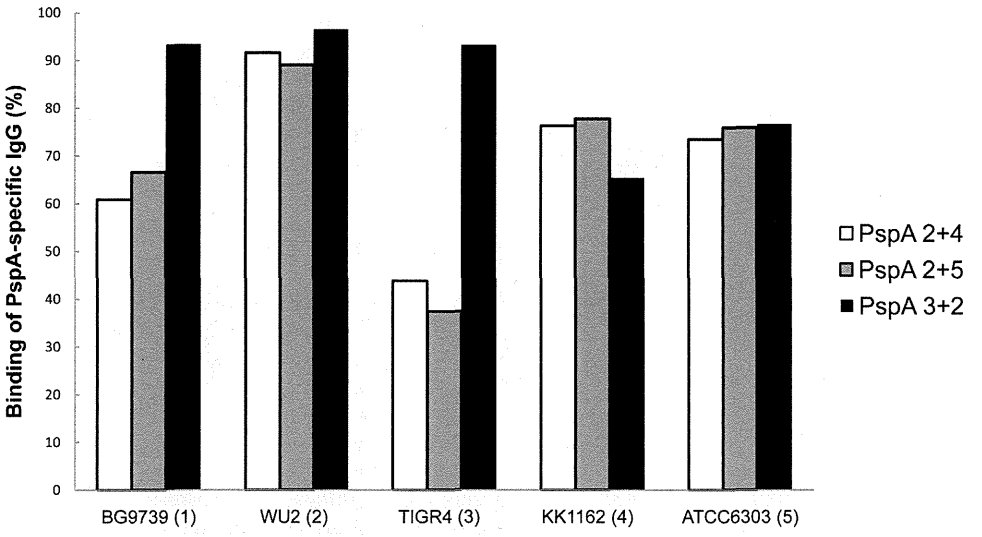

Fig. 3. The binding of PspA-specific IgG by antisera with PspA fusion proteins to the challenge strains with different clades. The mean percentages of fluorescent bacteria positive for IgG binding by antisera from mice immunized with PspA2+4, PspA2+5, or PspA3+2 in combination CpG ODNs plus AHG (double adjuvants) are shown for five pneumococcal strains with PspA clades 1–5 used in the challenge experiments. The numbers in parentheses represents the PspA clade.

3. Results

A schematic diagram of PspA and the three PspA fusion proteins constructed from PspA families 1 and 2 are shown in Fig. 1. The purified recombinant fusion proteins were electrophoresed on sodium dodecyl sulfate–polyacrylamide (SDS–PAGE) gels and evaluated by Coomassie blue staining (Fig. 2A) and by Western blotting using mouse anti-PspA/Rx1 sera (PspA/Rx1 and PspA/D39 are identical clade 2 PspA molecules) (Fig. 2B).

PspA-specific IgG binding >60% was found in antiserum raised by PspA2+4 or PspA2+5 plus double adjuvants for the challenge strains expressing PspA clades 1, 2, 4, and 5, but not for the strain expressing clade 3 (Fig. 3). By contrast, PspA-specific IgG binding > 60% was found for the challenge strains expressing all five PspA clades in antiserum raised by PspA3+2 plus double adjuvants.

For the challenge with the bacterial strain BG9739 with PspA clade 1, the survival rate was greater in mice immunized with PspA3+2 plus double adjuvants ($p < 0.01$) compared with mice

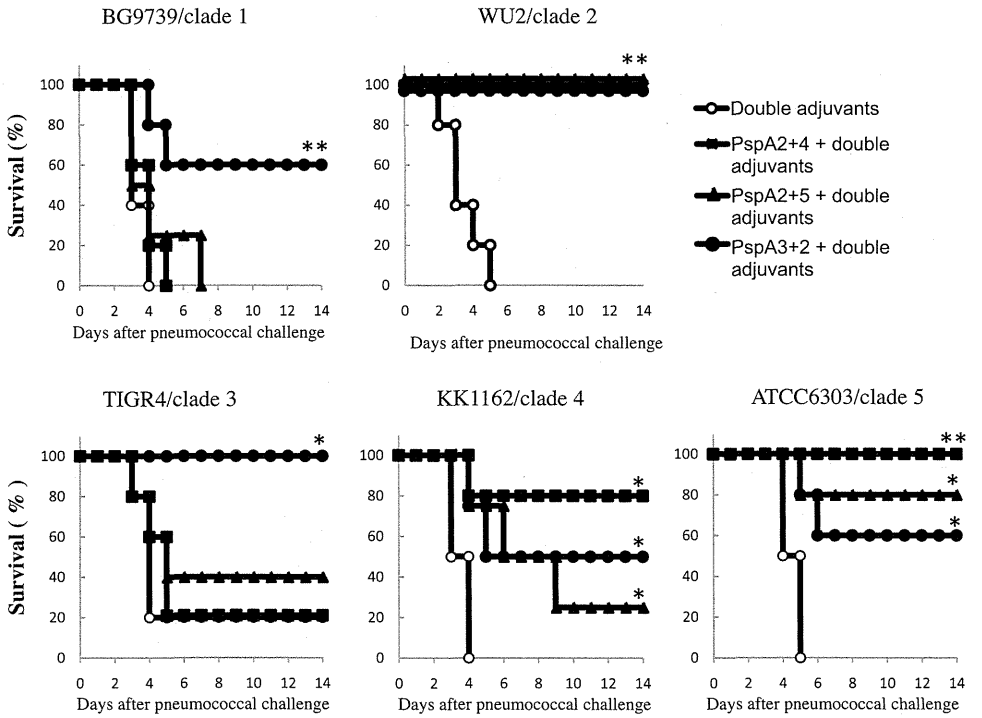

Fig. 4. Protective effects of immunization with fusion PspA proteins against pneumococcal challenge in mice. Mice were immunized subcutaneously with PspA2+4 (closed squares), PspA2+5 (closed triangles), or PspA3+2 (closed circles) in combination with CpG ODNs plus AHG (double adjuvants) or double adjuvants alone (open circles) three times at 1-week intervals. Two weeks after the last immunization, the immunized mice were challenged intranasally with pneumococcal strains with PspA clades 1–5. Mortality was monitored for 2 weeks. Eight to 10 mice per group were examined in each challenge experiment using pneumococcal strain with five different clades. *$p < 0.05$ (vs double adjuvants alone), **$p < 0.01$ (vs double adjuvants alone).

Table 1
Serotypes and PspA clades of 68 isolates from adults with invasive pneumococcal disease.

Serotype	No. strain	No. strain				
		Family 1		Family 2		
		Clade 1	Clade 2	Clade 3	Clade 4	Clade 5
1	1	1				
3	10	9		1		
4	4			4		
6A	2		1			1
6B	10	7		3		
6C	1		1			
7F	2			2		
9V	1			1		
10A	3	3				
11A	2				2	
12F	1			1		
14	5	5				
15A	1				1	
15B	1			1		
16	1			1		
18B	1	1				
18C	1	1				
19A	3			3		
19F	3	1		2		
20	1	1				
22F	3	3				
23A	1				1	
23F	5					5
33	1	1				
34	1	1				
35	2				2	
38	1		1			
Total 68 (100%)		34 (50%)	3 (4%)	19 (28%)	6 (9%)	6 (9%)

immunized with double adjuvants alone (Fig. 4). By contrast, the survival rate did not differ between mice immunized with PspA2+4 or PspA2+5 plus double adjuvants compared with mice immunized with double adjuvants alone. For the bacterial challenge with the WU2 strain with PspA clade 2, the survival rate was significantly higher in mice immunized with PspA2+4, PspA2+5, or PspA3+2 plus double adjuvants ($p < 0.01$) compared with mice immunized with double adjuvants alone. For the bacterial challenge with the TIGR4 strain with PspA clade 3, the survival rate was significantly higher in mice immunized with PspA3+2 plus double adjuvants ($p < 0.05$) compared with mice immunized with double adjuvants alone. The survival rate did not differ between mice immunized with PspA2+4 or PspA2+5 plus double adjuvants compared with mice immunized with double adjuvants alone. In the case of challenge with clade 4 and 5 strains, all three PspA fusion vaccines showed significant protection compared with mice immunized with double adjuvants alone ($p < 0.01$ or $p < 0.05$). These data indicate that immunization with the PspA3+2 vaccine conferred significant protection of mice against pneumococcal challenge by all of the strains expressing PspA clades 1–5. The other two PspA fusion proteins failed to elicit protection against two of the challenge strains (PspA clades 1 and 3).

The distribution of serotypes and PspA clades of 68 clinical isolates from adult patients with IPD are shown in Table 1. The major serotypes were serotype 3 (15%) and 6B (15%), followed by serotypes 14 (7%) and 23F (7%). The major PspA clades were clade 1 (50%) and clade 3 (28%), followed by clade 4 (9%), clade 5 (9%), and clade 2 (4%). All the clinical isolates belonged to PspA clades 1–5, which is in agreement with previous studies [6,13,25].

The binding of PspA-specific IgG in antiserum raised by PspA2+4, PspA2+5, or PspA3+2 plus double adjuvants was examined for the 68 clinical isolates (Fig. 5). The binding of PspA-specific IgG for clade 3 strains ($n = 19$) in antiserum raised by PspA3+2 was significantly higher than in that raised by PspA2+4 or PspA2+5 ($p < 0.05$). By contrast, the binding of PspA-specific IgG for clade 5 strains ($n = 6$) in antiserum raised by PspA3+2 was significantly lower than that by PspA2+4 ($p < 0.05$) or PspA2+5 ($p < 0.05$). No significant difference was found in the binding of PspA-specific IgG for 34 clade 1 strains, three PspA clade 2 strains, or six PspA clade 4 strains between the three types of antiserum raised by PspA2+4, PspA2+5, or PspA3+2.

4. Discussion

In this study, we have demonstrated >60% binding of PspA-specific IgG in the antiserum raised in mice by PspA2+4 or PspA2+5 to four challenge strains expressing clades 1, 2, 4, and 5, but low binding of PspA-specific IgG to the strain expressing clade 3 (Fig. 3). By contrast, >60% binding of PspA-specific IgG in antiserum raised in mice by PspA3+2 was found to all five challenge strains expressing PspA clades 1–5. Immunization with PspA3+2 provided significant protection against pneumococcal challenge by these five strains expressing clades 1–5, but PspA2+4 or PspA2+5 protected mice against only three of the strains expressing clades 2, 4 and 5 in this study (Fig. 4). Therefore, it may be speculated that the binding of PspA-specific IgG closely correlates with the protective effects of PspA fusion protein against pneumococcal challenge in mice. These findings are supported by a recent report on the ability of opsonophagocytic killing and protection of mice against pneumococcal infection by human antiserum to PspA [17]. Only one exception for this speculation is that no protection was found against pneumococcal challenge by the clade 1 strain BG9739 (serotype 4) in mice immunized with PspA2+4 or PspA2+5 plus double adjuvants despite of >60% binding of PspA-specific IgG in antiserum raised by PspA2+4 or PspA2+5 for this clade 1 strain. One possible reason for the inefficient immunization with PspA2+4 or PspA2+5 in mice infected with BG9739 strain may be the presence of serotype 4 capsular polysaccharide. Our previous study demonstrated that the difficulty in protecting against serotype 4 strains was eliminated when mice were immunized with a homologous PspA of the same PspA family [37]. However, only weak protection against infection with strain BG9739 was observed by immunization of mice with the homologous PspA clade 1 [28]. Therefore, it remains uncertain whether immunization with PspA2+4 or PspA2+5 plus double adjuvants did not protect against pneumococcal challenge by the clade 1 strain BG9739 in mice.

No differences were found in the binding of PspA-specific IgG to the clinical isolates belonging to the major clade 1 ($n = 34$) and the two minor clades 2 ($n = 3$) and 4 ($n = 6$) between the types of antiserum raised by the three PspA fusion proteins. For the clinical isolates belonging to the second major clade 3 ($n = 19$), antiserum raised by PspA3+2 demonstrated the greatest binding between the three types of antiserum raised by the PspA fusion proteins (Fig. 5). These findings are in agreement with those showing the binding of PspA-specific IgG to the TIGR4 strain expressing clade 3 for the three types of antiserum raised by each PspA fusion protein (Fig. 3). However, antiserum raised by PspA3+2 demonstrated the lowest binding to six clinical isolates belonging to the minor clade 5 between three types of antiserum raised by each PspA fusion protein. Collectively, PspA3+2 appears to be advantageous in terms of its cross-reactivity with clinical isolates and cross-protection against pneumococcal challenge in mice compared with the other two PspA fusion proteins.

Darrieux et al. reported that immunization with fusion proteins containing fragments of PspA from families 1 and 2 provided cross-protection against pneumococcal strains from families 1 and 2 in mice [30]. The fusion proteins containing PspA clade 1 and PspA clade 3 or 4 fragments provided significant protection against the A66.1 strain (PspA clades 1, and 2), but the protection against strains from clades 3 and 4 was of borderline significance. In another

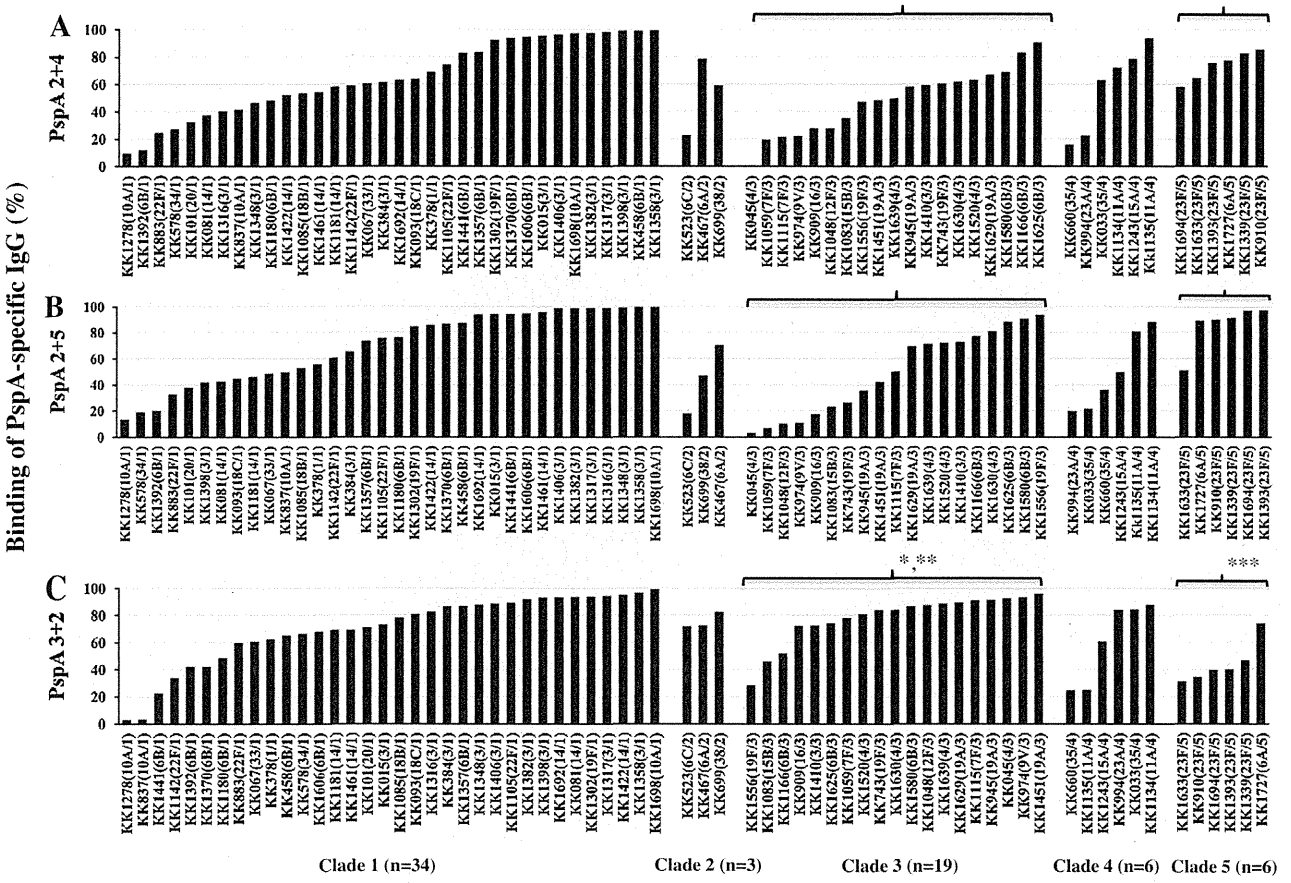

Fig. 5. Comparison of PspA-specific IgG binding by antisera with PspA2+4 (A), PspA2+5 (B), or PspA3+2 (C) in combination with CpG ODNs plus AHG (double adjuvants) to 68 pneumococcal isolates (34 for clade1, three for clade 2, 19 for clade 3, six for clade 4, and six for clade 5). The serotypes and PspA clades are shown in parentheses after the strain names. $^{*}p < 0.01$ (vs PspA2+4), $^{**}p < 0.05$ (vs PspA2+5), $^{***}p < 0.05$ (vs PspA2+4 or PspA2+5).

study, these authors reported that antiserum against fusion protein PspA1+4 demonstrated strong cross-reactivity with PspA clades 1 and 5 but low cross-reactivity with PspA clade 2 or 3 [29]. Consequently, Darrieux et al. failed to demonstrate significant protection against pneumococcal challenge by strains with PspA clades 1–5, although they demonstrated limited cross-protection by immunization with the fusion proteins containing fragments of PspA from families 1 and 2.

A limitation of our study is that we generated and examined only three PspA fusion proteins, which contained one clade each from PspA families 1 and 2. Another limitation is that the binding of PspA-specific IgG was assessed in a small number of clinical isolates from adult patients with IPD.

The antiserum raised by PspA3+2 demonstrated relatively weak binding capacity to the clinical isolates expressing PspA clade 5 in this study. Further studies are required to generate the other types of PspA fusion proteins that can induce PspA-specific IgG with a high affinity to strains expressing PspA clades 5, as well as to strains expressing PspA clade 1–4. In addition, immunization with PspA2+4 or PspA2+5 provided better protection than PspA3+2 against bacterial challenge of clade 4 or clade 5 strain in this study. Therefore, the combined immunization with PspA3+2 with PspA2+4 or PspA2+5 simultaneously or sequentially may have the potential to improve the breadth of immunity against pneumococcal isolates.

In conclusion, immunization of mice with PspA3+2 induced antiserum exhibiting a high binding capacity to the clinical isolates expressing PspA clades 1–4, but not clade 5. Among the three PspA fusion proteins examined in this study, PspA3+2 was found to be advantageous over the other two PspA fusion proteins because PspA3+2 induced a broad range of cross-reactivity with clinical isolates and afforded a cross-protection against pneumococcal challenge in mice.

Author contributions

K.O., Y.A., K.J.I., K.U. and K.T. conceived and designed the experiments. Z.P. and Y.A. performed the experiments. Z.P. and D.T. analyzed the data. K.O., Z.P., Y.A., and D.E.B. wrote the paper.

Conflict of interest statement

The authors declare no conflict of interest.

Acknowledgments

We thank Michiyo Hayakawa for technical assistance. This work was supported by the Program for Promotion of Fundamental Studies in Health Sciences of the National Institute of Biomedical Innovation and by the Biomedical Cluster Kansai project, which is promoted by the Regional Innovation Cluster Program and is subsidized by the Japanese Government; and by research grants from the Ministry of Health, Labor and Welfare of Japan.

Appendix A. Supplementary data

Supplementary data associated with this article can be found, in the online version, at http://dx.doi.org/10.1016/j.vaccine.2014.07.108.

References

[1] O'Brien KL, Wolfson LJ, Watt JP, Henkle E, Deloria-Knoll M, McCall N, et al. Burden of disease caused by *Streptococcus pneumoniae* in children younger than 5 years: global estimates. Lancet 2009;374:893–902.

[2] Pilishvili T, Lexau C, Farley MM, Hadler J, Harrison LH, Bennett NM, et al. Sustained reductions in invasive pneumococcal disease in the era of conjugate vaccine. J Infect Dis 2010;201:32–41.

[3] *Singleton RJ, Hennessy TW, Bulkow LR, Hammitt LL, Zulz T, Hurlburt DA, et al.* Invasive pneumococcal disease caused by nonvaccine serotypes among Alaska native children with high levels of 7-valent pneumococcal conjugate vaccine coverage. JAMA 2007;297:1784–92.

[4] Ardanuy C, Tubau F, Pallares R, Calatayud L, Domínguez MA, Rolo D, et al. Epidemiology of invasive pneumococcal disease among adult patients in Barcelona before and after pediatric 7-valent pneumococcal conjugate vaccine introduction, 1997–2007. Clin Infect Dis 2009;48:57–64.

[5] Miller E, Andrews NJ, Waight PA, Slack MPE, Gorge RC. Herd immunity and serotype replacement 4 years after seven-valent pneumococcal conjugate vaccination in England and Wales: an observation cohort study. Lancet Infect Dis 2011;11:760–8.

[6] Croney CM, Coats MT, Nahm MH, Briles DE, Crain MJ. PspA family distribution, unlike capsular serotype, remains unaltered following introduction of the heptavalent pneumococcal conjugate vaccine. Clin Vaccine Immunol 2012;19:891–6.

[7] Rev-Yochay G, Rahav G, Riesenberg K, Wiener-Well Y, Strahilevitz J, Stein M, et al. Initial effects of the national PCV7 childhood immunization program on adult invasive pneumococcal disease in Israel. PLOS ONE 2014;9:e88406.

[8] Briles DE, Tart RC, Swiatlo E, Dillard JP, Smith P, Benton KA, et al. Pneumococcal diversity: considerations for new vaccine strategies with emphasis on pneumococcal surface protein A (PspA). Clin Microbiol Rev 1998;11:645–57.

[9] Briles DE, Ades E, Paton JC, Sampson JS, Carlone GM, Huebner RC, et al. Intranasal immunization of mice with a mixture of the pneumococcal proteins PsaA and PspA is highly protective against nasopharyngeal carriage of *Streptococcus pneumoniae*. Infect Immun 2000;68:796–800.

[10] Ogunniyi AD, Folland RL, Briles DE, Hollingshead SK, Paton JC. Immunization of mice with combinations of pneumococcal virulence proteins elicits enhanced protection against challenge with *Streptococcus pneumoniae*. Infect Immun 2000;68:3028–33.

[11] Tai SS. *Streptococcus pneumoniae* protein vaccine candidates: properties, activities and animal studies. Crit Rev Microbiol 2006;32:139–53.

[12] *Daniels CC, Briles TC, Mirza S, Håkansson AP, Briles DE.* Capsule does not block antibody binding PspA, a surface virulence protein of *Streptococcus pneumoniae*. Microb Pathog 2006;40:228–33.

[13] Hollingshead SK, Baril L, Ferro S, King J, Coan P, Briles DE. Pneumococcal Proteins Epi Study Group. Pneumococcal surface protein A (PspA) family distribution among clinical isolates from adults over 50 years of age collected in seven countries. J Med Microbiol 2006;55:215–21.

[14] Tu A-H, Fulgham RL, McCrory MA, Briles DE, Szalai J. Pneumococcal surface protein A inhibits complement activation by *Streptococcus pneumoniae*. Infect Immun 1999;67:4720–4.

[15] Ren B, Szalai AJ, Hollingshead SK, Briles DE. Effects of PspA and antibodies to PspA on activation and deposition of complement on the pneumococcal surface. Infect Immun 2004;72:114–22.

[16] Briles DE, Hollingshead SK, King J, Swift A, Braun PA, Park MK, et al. Immunization of humans with recombinant pneumococcal surface protein A (rPspA) elicits antibodies that passively protect mice from fatal infection with *Streptococcus pneumoniae* bearing heterologous PspA. J Infect Dis 2000;182:1694–701.

[17] Daniels CC, Kim K-H, Burton RL, Mirza S, Walker M, King J, et al. Modified opsonization, phagocytosis, and killing assays to measure potentially protective antibodies against pneumococcal surface protein A. Clin Vaccine Immunol 2013;20:1549–58.

[18] Yother J, Briles DE. Structural properties and evolutionary relationships of PspA, a surface protein of *Streptococcus pneumoniae*, as revealed by sequence analysis. J Bacteriol 1992;174:601–9.

[19] Yother J, White JM. Novel surface attachment mechanism of the *Streptococcus pneumoniae* protein PspA. J Bacteriol 1994;176:2976–85.

[20] Senkovich O, Cook WJ, Mirza S, Hollingshead SK, Protasevich II, Briles DE, et al. Structure of a complex of human lactoferrin N-lobe with pneumococcal surface protein a provides insight into microbial defense mechanism. J Mol Biol 2007;370:701–13.

[21] McDaniel LS, Ralph BA, McDaniel DO, Briles DE. Localization of protection-eliciting epitopes on PspA of *Streptococcus pneumoniae* between amino acid residues 192 and 260. Microb Pathog 1994;17:323–37.

[22] Shaper M, Hollingshead SK, Benjamin Jr WH, Briles DE. PspA protects *Streptococcus pneumoniae* from killing by apolactoferrin, and antibody to PspA enhances killing of pneumococci by apolactoferrin. Infect Immun 2004;72:5031–40.

[23] Daniels CC, Coan P, King J, Hale J, Benton KA, Briles DE, et al. The proline-rich region of pneumococcal surface proteins A and C contains surface-accessible epitopes common to all pneumococci and elicits antibody-mediated protection against sepsis. Infect Immun 2010;78:2163–72.

[24] Hollingshead SK, Becker R, Briles DE. Diversity of PspA: mosaic genes and evidence for past recombination in *Streptococcus pneumoniae*. Infect Immun 2000;68:5889–900.

[25] Qian J, Yao K, Xue L, Xie G, Zheng Y, Wang C, et al. Diversity of pneumococcal surface protein A (PspA) and relation to sequence typing in *Streptococcus pneumonia* causing invasive diseases in Chinese children. Eur J Clin Microbiol Infect Dis 2012;31:217–23.

[26] Oma K, Zhao J, Ezoe H, Akeda Y, Koyama S, Ishi KJ, et al. Intranasal immunization with a mixture of PspA and a toll-like receptor agonist induces specific antibodies and enhances bacterial clearance in the airways of mice. Vaccine 2009;27:3181–8.

[27] Moreno AT, Oliveira ML, Ferreira DM, Ho PL, Darrieux M, Leite LC, et al. Immunization of mice with single PspA fragments induces antibodies capable of mediating complement deposition on different pneumococcal strains and cross-protection. Clin Vaccine Immunol 2010;17:439–46.

[28] Briles DE, Hollingshead SK, Nabors GS, Paton JC, Brooks-Water A. The potential for using protein vaccines to protect against otitis media caused by *Streptococcus pneumoniae*. Vaccine 2000;19(Suppl. 1):S87–95.

[29] Darrieux M, Moreno AT, Ferreira DM, Pimenta FC, de Andrade AL. Recognition of pneumococcal isolates by antisera raised against PspA fragments from different clades. J Med Microbiol 2008;57:273–8.

[30] Darrieux M, Miyaji EN, Ferreira DM, Lopes LM, Lopes A, Ren B, et al. Fusion proteins containing family 1 and family 2 PspA fragments elicit protection against *Streptococcus pneumoniae* that correlates with antibody-mediated enhancement of complement deposition. Infect Immun 2007;75:5930–8.

[31] Xin W, Li Y, Mo H, Roland KL, Curtiss III R. PspA family fusion proteins delivered by attenuated *Salmonella enterica* serovar Typhimilium extend and enhance protection against *Streptococcus pneumoniae*. Infect Immun 2009;77:4518–28.

[32] Chiba N, Morozumi M, Shouji M, Wajima T, Iwata S, Sunakawa K, et al. Rapid decrease of 7-valent conjugate vaccine coverage for invasive pneumococcal diseases in pediatric patients in Japan. Microb Drug Resist 2013;19:308–15.

[33] *Pimenta FC, Ribeiro-Dias F, Brandileone MC, Miyaji EN, Leite LC, Sgambatti de Andrade AL.* Genetic diversity of PspA types among nasopharyngeal isolates collected during an ongoing surveillance study of children in Brazil. J Clin Microbiol 2006;44:279–84.

[34] Ezoe H, Akeda Y, Piao Z, Aoshi T, Koyama S, Tanimoto T, et al. Intranasal vaccination with pneumococcal surface protein A plus poly(I:C) protects against secondary pneumococcal pneumonia in mice. Vaccine 2011;29:1754–61.

[35] Takeshita F, Leifer CA, Gursel I, Ishii KJ, Takeshita S, Gursel M, et al. Cutting edge: role of Toll-like receptor 9 in CpG DNA-induced activation of human cells. J Immunol 2001;167:3555–8.

[36] Tougan T, Aoshi T, Coban C, Katakai Y, Kai C, Yasumoti Y, et al. TLR9 adjuvants enhance immunogenicity and protective efficacy of the SE36/AHG malaria vaccine in nonhuman primate models. Hum Vaccine Immunother 2013;9:283–90.

[37] Roche H, Ren B, McDaniel LS, Håkansson A, Briles DE. Relative roles of genetic background and variation in PspA in the ability of antibodies to PspA to protect against capsular type 3 and 4 strains of *Streptococcus pneumoniae*. Infect Immun 2003;71:4498–505.

Vaccine 32 (2014) 5295–5300

Contents lists available at ScienceDirect

Vaccine

journal homepage: www.elsevier.com/locate/vaccine

Hemozoin as a novel adjuvant for inactivated whole virion influenza vaccine

Ryuta Uraki[a], Subash C. Das[b], Masato Hatta[b], Maki Kiso[a], Kiyoko Iwatsuki-Horimoto[a], Makoto Ozawa[c,d], Cevayir Coban[e], Ken J. Ishii[f,g], Yoshihiro Kawaoka[a,b,h,i,*]

[a] Division of Virology, Department of Microbiology and Immunology, Institute of Medical Science, University of Tokyo, Tokyo 108-8639, Japan
[b] Influenza Research Institute, Department of Pathobiological Sciences, University of Wisconsin-Madison, Madison, WI 53711, USA
[c] Laboratory of Animal Hygiene, Joint Faculty of Veterinary Medicine, Kagoshima University, Kagoshima 890-0065, Japan
[d] Transboundary Animal Diseases Center, Joint Faculty of Veterinary Medicine, Kagoshima University, Kagoshima 890-0065, Japan
[e] Laboratory of Malaria Immunology, Immunology Frontier Research Center (IFReC), Osaka University, Osaka, Japan
[f] Laboratory of Adjuvant Innovation, National Institute of Biomedical Innovation, Osaka, Japan
[g] Laboratory of Vaccine Science, IFReC, Osaka University, Osaka, Japan
[h] ERATO Infection-Induced Host Responses Project (JST), Saitama 332-0012, Japan
[i] Department of Special Pathogens, International Research Center for Infectious Diseases, Institute of Medical Science, University of Tokyo, Minato-ku, Tokyo 108-8639, Japan

ARTICLE INFO

Article history:
Received 31 January 2014
Received in revised form 27 May 2014
Accepted 22 July 2014
Available online 6 August 2014

Keywords:
Influenza virus
Vaccine
Hemozoin
Adjuvant
Antibody

ABSTRACT

Because vaccination is an effective means to protect humans from influenza viruses, extensive efforts have been made to develop not only new vaccines, but also for new adjuvants to enhance the efficacy of existing inactivated vaccines. Here, we examined the adjuvanticity of synthetic hemozoin, a synthetic version of the malarial by-product hemozoin, on the vaccine efficacy of inactivated whole influenza viruses in a mouse model. We found that mice immunized twice with hemozoin-adjuvanted inactivated A/California/04/2009 (H1N1pdm09) or A/Vietnam/1203/2004 (H5N1) virus elicited higher virus-specific antibody responses than did mice immunized with non-adjuvanted counterparts. Furthermore, mice immunized with hemozoin-adjuvanted inactivated viruses were better protected from lethal challenge with influenza viruses than were mice immunized with non-adjuvanted inactivated vaccines. Our results show that hemozoin improves the immunogenicity of inactivated influenza viruses, and is thus a promising adjuvant for inactivated whole virion influenza vaccines.

1. Introduction

Despite the worldwide surveillance network of influenza viruses, the incidence and prevalence of influenza are hard to predict, as exemplified by the influenza (H1N1) 2009 pandemic [1,2]. Vaccination stands on the frontlines of influenza infection control: both live attenuated and inactivated influenza vaccines are currently available [3,4]. The live attenuated vaccines are more efficient than inactivated vaccines at inducing the mucosal immune responses that play an important role in combating influenza virus infection [5,6]. However, because of the safety concerns such as the emergence of revertant and/or reassortant viruses, these live vaccines are licensed in a limited number of countries. By contrast, inactivated vaccines have few safety concerns and are globally available. While they efficiently induce humoral immune responses, a high dose (usually 15 μg) of the inactivated vaccine is required to provide adequate immunity [7,8]. Therefore, there is room for improvement in the current influenza vaccines.

Vaccine is generally assessed on the basis of immunogenicity, safety, and costs [9]. To enhance the immunogenicity of the inactivated vaccines, adjuvants, such as aluminum compounds and salts, have been considered [10]. Adjuvants are defined as immune modulators that are added to inactivated vaccines to boost the immune responses, enable the use of lower amounts of antigens, and thus expand the vaccine supply [10,11]. Although most of the inactivated influenza vaccines currently used are injected via the intramuscular or subcutaneous routes, previous studies have shown that intranasal vaccinations induce antibodies more effectively than do intramuscular or subcutaneous vaccinations [12–14]. However, the

* Corresponding author at: Division of Virology, Department of Microbiology and Immunology, Institute of Medical Science, University of Tokyo, 4-6-1, Shirokanedai, Minato-ku, Tokyo, Japan. Tel.: +81 3 5449 5504; fax: +81 3 5449 5408.
E-mail addresses: kawaoka@ims.u-tokyo.ac.jp, kawaokay@svm.vetmed.wisc.edu (Y. Kawaoka).

http://dx.doi.org/10.1016/j.vaccine.2014.07.079
0264-410X/

alum compounds that are generally used as adjuvants for intramuscular administration do not enhance the efficacy of intranasal vaccines; therefore, to improve the efficacy of intranasal vaccines, novel intranasal adjuvants are required [15].

Malaria parasites digest hemoglobin in red blood cells, resulting in the production of potentially toxic heme metabolites [16]. To protect themselves from oxidative damage, the parasites polymerize toxic heme enzymatically into a safer insoluble substance, hemozoin [17]. Recently, hemozoin and a chemically identical synthetic version of hemozoin (called β-hematin) have been investigated for their potency as novel adjuvants, and the molecular pathway underlying their immunological function has also been studied. Such studies have demonstrated that purified hemozoin is a non-DNA ligand for Toll-like receptor 9 (TLR9) that may activate innate immune cells via TLR9 [18–20]. This latter point has been a subject of debate, however, because the adjuvant effect of synthetic hemozoin is dependent on MyD88 and not TLR9 [21]. Recently, we reported that hemozoin enhances the protective efficacy of a subcutaneously administered influenza HA split vaccine in a ferret model [22].

We speculated that synthetic hemozoin (hereafter referred to only as hemozoin) could serve as a novel intranasal adjuvant for the inactivated influenza vaccine. Accordingly, here we evaluated the adjuvanticity of hemozoin on the vaccine efficacy of intranasally administered inactivated whole virion influenza vaccines in a murine lethal infection model. The results indicate that hemozoin is a promising adjuvant for inactivated whole virion influenza vaccines.

2. Materials and methods

2.1. Cells and viruses

Human embryonic kidney HEK293T cells were maintained in Dulbecco's modified Eagle medium (Lonza, Basel, Switzerland) supplemented with 10% fetal calf serum (Invitrogen, Carlsbad, CA). Madin-Darby canine kidney (MDCK) cells were maintained in minimum essential medium (MEM) (Invitrogen) supplemented with 5% newborn calf serum (NCS) (Sigma, St. Louis, MO). All cells were maintained in a humidified incubator at 37 °C in 5% CO_2.

A/California/04/2009 (H1N1; Ca04), which is an early isolate of influenza (H1N1) 2009 pandemic viruses, and mouse-adapted Ca04 (MACa04) [23] viruses were propagated in MDCK cells as previously described [24]. A/Vietnam/1203/2004 (H5N1; VN1203) virus, a representative strain of highly pathogenic avian influenza viruses, was grown in MDCK cells and in 10-day-old embryonated chicken eggs to use as challenge viruses and as vaccine and ELISA antigens, respectively. All work involving live VN1203 virus was carried out at the ABSL-3 laboratory of the Influenza Research Institute, UW-Madison, following the protocol designed by Institutional Animal Care and Use Committee (IACUC).

2.2. Inactivated influenza virus and adjuvant

To inactivate MDCK cell-propagated Ca04 virus and egg-propagated VN1203 virus, formalin (final concentration, 0.1%) was added to the viruses, which were then incubated at 4 °C for 1 week. The inactivated viruses were purified through a 10–50% sucrose density gradient and resuspended in phosphate-buffered saline (PBS) as described previously [25]. Inactivation of Ca04 viruses was confirmed by passaging them twice in MDCK cells and examining their cytopathic effect; inactivation of VN1203 viruses was confirmed by passaging them twice in embryonated chicken eggs followed by hemagglutination assays.

Synthetic hemozoin, was purified from hemin chloride (>98% pure, Fluka) by using the acid-catalyzed method described previously [21] and was re-suspended in endotoxin-free water with no detectable levels of endotoxin. The synthetic hemozoin concentration was calculated in mM (1 mg of hemozoin in 1 ml of water was equal to 1 mM).

2.3. Immunization and protection studies

For the immunization and protection studies with Ca04 virus, six-week-old female BALB/c mice ($n = 13$ per group) were anesthetized with isoflurane and intranasally administered with 50 μl of PBS, 9 mM hemozoin only, inactivated Ca04 only [5×10^6 plaque-forming unit (PFU), which corresponds to 0.1 μg when the total amount of viral protein was measured by using a BCA protein assay (Thermo Scientific)], or inactivated Ca04 adjuvanted with 9 mM hemozoin, twice with a 2-week interval between the immunizations. Three weeks after the final administration, three mice from each group were euthanized for collection of bronchoalveolar lavage fluid (BALF) and nasal washes. The remaining mice ($n = 10$ per group) were intranasally challenged with 10-fold 50% mouse lethal doses (MLD_{50}) of MACa04 virus. On days 3 and 6 post-challenge, three mice each were euthanized and their lungs were collected, homogenized with MEM containing 0.3% BSA, and examined for virus titers by using plaque assays in MDCK cells. The body weight and survival of the remaining challenged mice ($n = 4$ per group) were monitored daily for 14 days.

For VN1203 virus, four-week-old female BALB/c mice ($n = 16$ per group) were immunized as described above. Two weeks after the last immunization, five mice from each group were euthanized for collection of BALF and nasal washes. The remaining mice ($n = 11$ per group) were challenged with 100 MLD_{50} of VN1203 virus. On days 3 and 6 post-challenge, three mice each were euthanized and their lungs were collected, homogenized with MEM containing 0.3% BSA, and examined for virus titers by using plaque assays in MDCK cells. The body weight and survival of the remaining challenged mice ($n = 5$ per group) were monitored daily for 14 days.

2.4. Detection of virus-specific antibodies

Virus-specific antibodies in nasal washes, BALF, and serum were detected by using an ELISA as previously described [25–27]. Briefly, 96-well ELISA plate wells were coated with approximately 0.3 μg (in 50 μl) of purified Ca04 or VN1203 virus treated with disruption buffer (0.5 M Tris–HCl [pH 8.0], 0.6 M KCl, and 0.5% Triton X-100) or sarkosyl, respectively. After incubation of the virus-coated plates with the test samples, virus-specific IgA and IgG antibodies in the samples were detected by using anti-mouse IgA and IgG goat antibodies conjugated to horseradish peroxidase (Kirkegaard & Perry Laboratory Inc., Gaithersburg, MD, Rockland), respectively.

2.5. Hemagglutination inhibition assay (HI assay)

To detect HI antibodies against Ca04 and VN1203, an HI assay was performed as described previously [28,29]. Briefly, serum samples were treated with receptor-destroying enzyme (RDE; Denka Seiken Co., Ltd.) by incubating at 37 °C for 16–18 h followed by inactivation at 56 °C for 30 min. One volume of turkey or horse red blood cells (RBCs) was then added to 20 volumes of serum and the sera were incubated for 1 h on ice with intermittent mixing. The samples were then centrifuged at 900 × g for 5 min, and the supernatants were transferred to new tubes for use in the HI assay. Serially diluted sera (2-fold dilutions) were mixed with 4 HA units of virus antigen and incubated with 0.5% turkey RBCs or 1% horse RBCs to determine the extent of hemagglutination inhibition.

2.6. Statistical analysis

Statistically significant differences in the virus-specific titers ($P < 0.05$ and $P < 0.01$) and the survival rates of the challenged mice ($P < 0.05$) were assessed by use of a one-way ANOVA followed by a Dunnett's test and Log-rank statistical analysis, respectively.

3. Results

3.1. Hemozoin enhances influenza virus-specific antibody responses in mice

To examine the effect of hemozoin on antibody responses elicited by immunization with inactivated influenza viruses, we intranasally administered BALB/c mice with hemozoin-adjuvanted inactivated virus (Ca04 or VN1203 virus, 5×10^6 plaque-forming units (PFU), the total amount of viral protein was 0.1 μg) twice with a 2-week interval between the immunizations. At three or two weeks after the final administration, we examined the antibody responses to the administered Ca04 or VN1203 virus by using an ELISA to measure the amount of IgG in the serum and IgA in the BALF and nasal washes (Fig. 1). Neither IgG nor IgA against Ca04 or VN1203 virus was appreciably detected in any samples from the PBS- or hemozoin-administered mice. Under these conditions, although one mouse immunized with non-adjuvanted inactivated Ca04 (Fig. 1A upper panel) and one mouse immunized with non-adjuvanted inactivated VN1203 virus (Fig. 1B upper panel) produced virus-specific IgG in the serum at a detectable level, all of the mice immunized with hemozoin-adjuvanted inactivated Ca04 ($n = 3$) or VN1203 ($n = 5$) virus elicited significantly higher levels of virus-specific IgG in the serum. We also examined the functional properties of the elicited antibodies by using hemagglutination inhibition (HI) assays. For both the Ca04 and VN1203 viruses, greater HI titers were obtained after vaccination with hemozoin-adjuvanted inactivated viruses than with non-adjuvanted inactivated viruses (Fig. 1A and B upper, right panel), although the titer difference for Ca04 virus between the hemozoin group and the control groups was not statistically significant (Fig. 1A upper, right panel). Of note, although the addition of hemozoin did not enhance IgA production in the nasal washes or BALF of the inactivated Ca04 virus-immunized mice, some of the mice immunized with the hemozoin-adjuvanted inactivated VN1203 virus did produce high levels of virus-specific IgA in their nasal washes and BALF (Fig. 1B lower panels). Taken together, these results indicate that hemozoin enhanced the immunogenicity of inactivated influenza viruses, resulting in more efficient production of virus-specific antibodies.

3.2. Hemozoin enhances the efficacy of inactivated influenza vaccine against lethal challenge in mice

To further assess the adjuvanticity of hemozoin, mice immunized twice with hemozoin-adjuvanted inactivated Ca04 or VN1203 virus were challenged with a lethal dose of MACa04 (10 MLD_{50}) [23] or VN1203 (100 MLD_{50}) virus (Fig. 2). In the MACa04 challenge group, although all of the PBS-administered mice and 75% of the hemozoin-administered or inactivated Ca04 virus-immunized mice died, all of the mice immunized with hemozoin-adjuvanted inactivated Ca04 virus survived (Fig. 2A). Intriguingly, no significant difference was found in Ca04 virus titers in the lungs among the mouse groups tested (Table 1). These results suggest that the adjuvanticity of hemozoin was sufficient to protect mice from lethal challenge with MACa04 virus.

For VN1203 virus, all PBS- and hemozoin-administered and inactivated VN1203 virus-immunized mice died following the lethal challenge (Fig. 2B). By contrast, 60% of the mice immunized with hemozoin-adjuvanted inactivated VN1203 virus survived although mice of all groups experienced body weight loss (Fig. 2B). In accordance with the results of the MACa04 virus challenge, the addition of hemozoin to inactivated VN1203 virus immunization did not affect the virus titers in the lungs of VN1203 virus-challenged mice (Table 2). These results suggest that hemozoin enhanced the vaccine efficacy of the inactivated influenza viruses by modulating host responses, but not by directly inhibiting virus replication. Overall, these results suggest that hemozoin is a promising adjuvant for inactivated influenza vaccines.

Table 1
Virus titers in the lungs of immunized mice challenged with mouse-adapted Ca04 virus.[a]

Immunization	Day after challenge	Virus titer (mean $\log_{10}$ PFU ± SD/g) in: lungs
PBS	3	8.1 ± 0.03
	6	6.5 ± 0.3
Hemozoin	3	8.2 ± 0.03
	6	6.6 ± 0.06
Inactivated Ca04 virus	3	8.1 ± 0.2
	6	5.7 ± 1.0
Hemozoin-adjuvanted inactivated Ca04 virus	3	8.0 ± 0.2
	6	6.2 ± 0.4

[a] Mice were intranasally immunized twice with the indicated agents (50 μl per mouse) and challenged with 10 MLD_{50} of MACa04 virus (50 μl per mouse) 3 weeks after the final immunization. Lungs were collected from mice ($n = 3$) on days 3 and 6 after challenge and examined for virus titers by use of plaque assays in MDCK cells.

Table 2
Virus titers in the lungs of immunized mice challenged with VN1203 virus.[a]

Immunization	Day after challenge	Virus titer (mean $\log_{10}$ PFU ± SD/g) in: lungs
PBS	3	6.3 ± 0.2
	6	6.3 ± 0.2
Hemozoin	3	6.6 ± 0.2
	6	6.3 ± 0.2
Inactivated VN1203 virus	3	6.7 ± 0.3
	6	5.6 ± 0.4
Hemozoin-adjuvanted inactivated VN1203 virus	3	6.4 ± 0.3
	6	6.0 ± 0.4

[a] Mice were intranasally immunized twice with the indicated agents (50 μl per mouse) and challenged with 100 MLD_{50} of VN1203 virus (50 μl per mouse) 4 weeks after the final immunization. Lungs were collected from mice ($n = 3$) on days 3 and 6 after challenge and examined for virus titers by use of plaque assays in MDCK cells.

4. Discussion

Here, we examined the effect of an adjuvant candidate, hemozoin, on the vaccine efficacy of inactivated whole virion influenza vaccines against lethal challenge in a mouse model. Significantly better virus-specific antibody responses were induced by hemozoin-adjuvanted inactivated virus than by inactivated viruses (Fig. 1). We further demonstrated that the hemozoin-adjuvanted inactivated viruses protected mice from lethal challenges more efficiently than did their non-adjuvanted counterparts with no effect of virus titers in the lungs (Fig. 2, Tables 1 and 2). These results indicate that hemozoin is a promising candidate as an effective adjuvant for inactivated whole virion influenza vaccines.

We observed significantly higher levels of IgA specific for VN1203 virus in the BALF and nasal washes, and of serum IgG, in mice immunized with hemozoin-adjuvanted inactivated VN1203 virus than in mice immunized with non-adjuvanted inactivated VN1203 virus-immunized mice (Fig. 1B). These results suggest that hemozoin enhanced the mucosal immune responses and

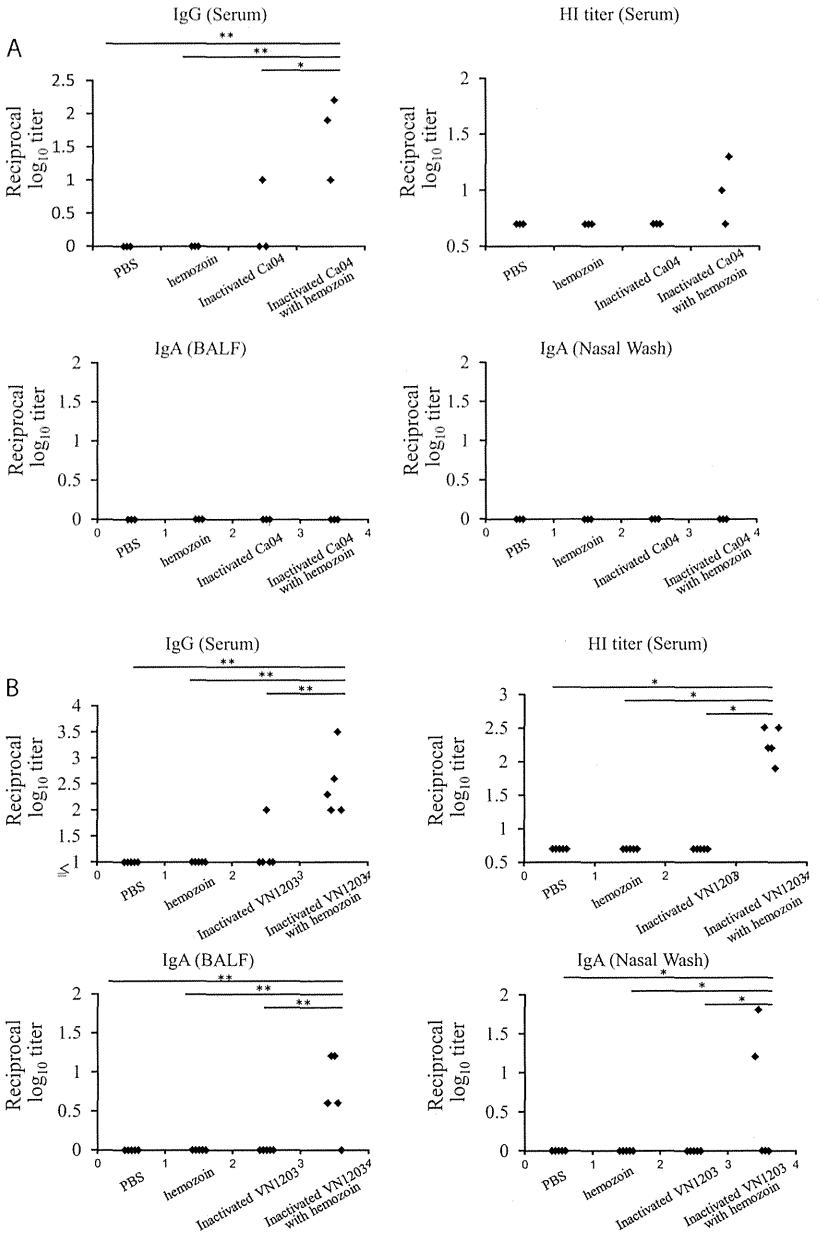

Fig. 1. Virus-specific antibody responses in immunized mice. Virus-specific antibodies were detected by means of ELISA and HI assays with purified Ca04 (A) or VN1203 (B) virus as a viral antigen. IgG antibody titers (upper, left panels) and HI titers (upper, right panels) in serum and IgA antibody titers in the BALF (lower, left panels), and nasal washes (lower, right panels) from mice intranasally mock-immunized with PBS or hemozoin or immunized with non-adjuvanted or hemozoin-adjuvanted inactivated virus were measured. Values represent antibody titers in individual mice (A: $n=3$, B: $n=5$). Statistically significant differences (*: $P<0.05$, **: $P<0.01$) are indicated.

may potentially compensate for the well-recognized weakness of inactivated vaccines [30,13,31]. By contrast, enhanced IgA production by the hemozoin addition was not observed with the Ca04 virus counterparts (Fig. 1A). This contradiction may reflect a difference in immunogenicity between the Ca04 and VN1203 viruses. Further study is required to clarify the mechanisms by which hemozoin promotes IgA responses after immunization with inactivated vaccines. In addition, hemozoin-adjuvanted inactivated virus protected mice better than non-adjuvanted inactivated viruses although virus titers in lungs were similar between animals immunized with and without the adjuvant (Fig. 2, Tables 1 and 2). This finding suggests that hemozoin enhanced the vaccine efficacy of the inactivated influenza viruses by modulating host responses. In the current study, we measured viral loads only in respiratory organs, which are the primary sites of influenza virus replication even for strains that cause systemic infection (e.g., VN1203 virus). A further study to examine the inhibitory effect of hemozoin on systemic spread of influenza viruses may explain the better protection afforded by hemozoin-adjuvanted vaccine.

Although hemozoin is a ligand for TLR9 [18–20], studies using TLR9- or MyD88-deficient mice suggest that the potent adjuvant effect of synthetic hemozoin is mediated not via TLR9, but through MyD88 [21]. In addition, previous studies have demonstrated that hemozoin stimulates innate inflammatory responses, inducing neutrophil recruitment via MyD88 [21,32]. Thus, one of the possible mechanisms underlying the hemozoin-mediated enhanced efficacy of inactivated influenza vaccine may be that hemozoin induces the balanced Th1/Th2 responses in a MyD88-dependent manner, leading to the improved immunogenicity of the inactivated influenza viruses and to the better protection against lethal challenge with influenza viruses. Of note, one of four mice administered with only hemozoin survived after the lethal challenge with

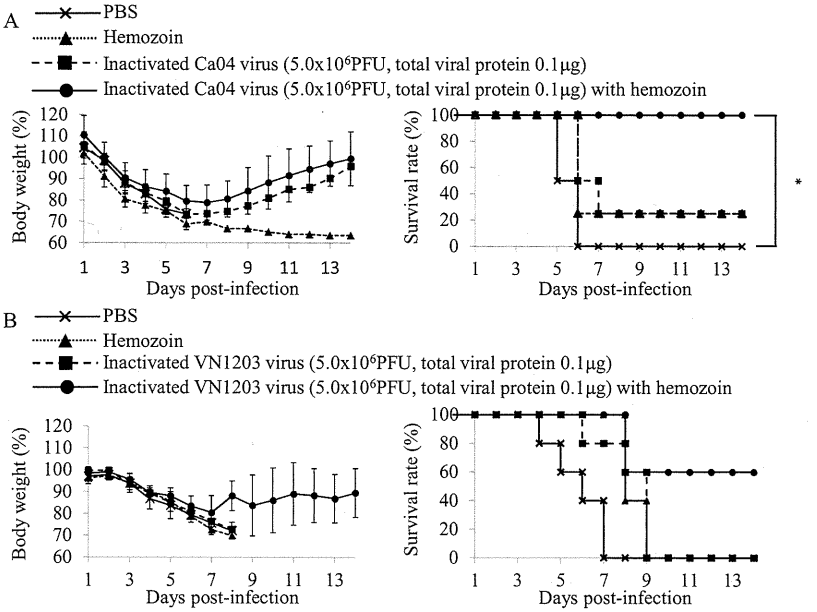

Fig. 2. Body weight changes and survival of mice challenged with lethal doses of viruses. Mice were mock-immunized with PBS or hemozoin, or immunized with non-adjuvanted or hemozoin-adjuvanted inactivated virus twice with a 2-week interval in between the immunizations. Three or four weeks after the final immunization, mice were intranasally challenged with 10 MLD_{50} of MACa04 virus (A: $n=4$) or 100 MLD_{50} of VN1203 virus (B: $n=5$), respectively. Body weight (left panels) and survival (right panels) were monitored for 14 days after challenge. Values are expressed as mean changes in body weight ± SD (left panels). Statistically significant differences in the survival rate of immunized mice (*: $P<0.05$) are indicated (A: right panel).

MACa04 virus (Fig. 2A), suggesting that hemozoin itself might have protective effects against influenza virus infection. Additional study is required to clarify the inhibitory effect of hemozoin on influenza virus infection.

In conclusion, here, we demonstrated the potential of hemozoin as a novel whole virion influenza vaccine adjuvant. Because the mechanism by which hemozoin enhances immunogenicity remains unclear, we should continue to evaluate the adjuvanticity of hemozoin in the context of influenza vaccination. In addition, to establish the efficacy of hemozoin as an adjuvant, further studies are needed including studies in an additional animal model such as ferrets.

Acknowledgements

We thank Dr. Susan Watson for editing the manuscript and Y. Igari and T. Tsukui from Nihon Zenoaq, Co., Ltd. for providing synthetic hemozoin. This work was supported, by a Grant-in-Aid for Specially Promoted Research, by the Japan Initiative for the Global Research Network on Infectious Diseases from the Ministry of Education, Culture, Sports, Science, and Technology, Japan, by grants-in-aid from the Ministry of Health, Labour, and Welfare, Japan, by ERATO (Japan Science and Technology Agency), by Strategic Basic Research Programs of Japan Science and Technology Agency, by National Institute of Allergy and Infectious Diseases Public Health Service research grants, and by an NIAID-funded Center for Research on Influenza Pathogenesis (CRIP, HHSN266200700010C). R.U. is supported by JSPS Research Fellowships for young scientists.

References

[1] Glezen WP. Cold-adapted, live attenuated influenza vaccine. Expert Rev Vaccines 2004;3(April (2)):131–9.
[2] Neumann G, Kawaoka Y. The first influenza pandemic of the new millennium. Influenza Other Respir Viruses 2011;5(May (3)):157–66.
[3] Nabel GJ, Fauci AS. Induction of unnatural immunity: prospects for a broadly protective universal influenza vaccine. Nat Med 2010;16(December (12)):1389–91.
[4] Lambert LC, Fauci AS. Influenza vaccines for the future. N Engl J Med 2010;363(November (21)):2036–44.
[5] Rimmelzwaan GF, Fouchier RA, Osterhaus AD. Influenza virus-specific cytotoxic T lymphocytes: a correlate of protection and a basis for vaccine development. Curr Opin Biotechnol 2007;18(December (6)):529–36.
[6] Cox RJ, Brokstad KA, Ogra P. Influenza virus: immunity and vaccination strategies. Comparison of the immune response to inactivated and live, attenuated influenza vaccines. Scand J Immunol 2004;59(January (1)):1–15.
[7] Brokstad KA, Cox RJ, Olofsson J, Jonsson R, Haaheim LR. Parenteral influenza vaccination induces a rapid systemic and local immune response. J Infect Dis 1995;171(January (1)):198–203.
[8] Cox RJ, Brokstad KA, Zuckerman MA, Wood JM, Haaheim LR, Oxford JS. An early humoral immune response in peripheral blood following parenteral inactivated influenza vaccination. Vaccine 1994;12(August (11)):993–9.
[9] Tetsutani K, Ishii KJ. Adjuvants in influenza vaccines. Vaccine 2012;30(December (52)):7658–61.
[10] Reed SG, Orr MT, Fox CB. Key roles of adjuvants in modern vaccines. Nat Med 2013;19(December (12)):1597–608.
[11] Dey AK, Srivastava IK. Novel adjuvants and delivery systems for enhancing immune responses induced by immunogens. Expert Rev Vaccines 2011;10(February (2)):227–51.
[12] van Riet E, Ainai A, Suzuki T, Hasegawa H. Mucosal IgA responses in influenza virus infections; thoughts for vaccine design. Vaccine 2012;30(August (40)):5893–900.
[13] Tumpey TM, Renshaw M, Clements JD, Katz JM. Mucosal delivery of inactivated influenza vaccine induces B-cell-dependent heterosubtypic cross-protection against lethal influenza A H5N1 virus infection. J Virol 2001;75(June (11)):5141–50.
[14] Ainai A, Tamura S, Suzuki T, Ito R, Asanuma H, Tanimoto T, et al. Characterization of neutralizing antibodies in adults after intranasal vaccination with an inactivated influenza vaccine. J Med Virol 2012;84(February (2)):336–44.
[15] Petrovsky N, Aguilar JC. Vaccine adjuvants: current state and future trends. Immunol Cell Biol 2004;82(October (5)):488–96.
[16] Francis SE, Sullivan Jr DJ, Goldberg DE. Hemoglobin metabolism in the malaria parasite *Plasmodium falciparum*. Annu Rev Microbiol 1997;51:97–123.
[17] Arese P, Schwarzer E. Malarial pigment (haemozoin): a very active 'inert' substance. Ann Trop Med Parasitol 1997;91(July (5)):501–16.
[18] Coban C, Ishii KJ, Kawai T, Hemmi H, Sato S, Uematsu S, et al. Toll-like receptor 9 mediates innate immune activation by the malaria pigment hemozoin. J Exp Med 2005;201(January (1)):19–25.
[19] Parroche P, Lauw FN, Goutagny N, Latz E, Monks BG, Visintin A, et al. Malaria hemozoin is immunologically inert but radically enhances innate responses by presenting malaria DNA to Toll-like receptor 9. Proc Natl Acad Sci U S A 2007;104(February (6)):1919–24.
[20] Wu X, Gowda NM, Kumar S, Gowda DC. Protein–DNA complex is the exclusive malaria parasite component that activates dendritic cells and triggers innate immune responses. J Immunol 2010;184(April (8)):4338–48.

[21] Coban C, Igari Y, Yagi M, Reimer T, Koyama S, Aoshi T, et al. Immunogenicity of whole-parasite vaccines against *Plasmodium falciparum* involves malarial hemozoin and host TLR9. Cell Host Microbe 2010;7(January (1)): 50–61.
[22] Onishi M, Kitano M, Taniguchi K, Homma T, Kobayashi M, Sato A, et al. Hemozoin is a potent adjuvant for hemagglutinin split vaccine without pyrogenicity in ferrets. Vaccine 2014;32(May (25)):3004–9.
[23] Sakabe S, Ozawa M, Takano R, Iwastuki-Horimoto K, Kawaoka Y. Mutations in PA, NP, and HA of a pandemic (H1N1) 2009 influenza virus contribute to its adaptation to mice. Virus Res 2011;158(June (1–2)):124–9.
[24] Yamada S, Hatta M, Staker BL, Watanabe S, Imai M, Shinya K, et al. Biological and structural characterization of a host-adapting amino acid in influenza virus. PLoS Pathog 2010;6(8):e1001034.
[25] Uraki R, Kiso M, Iwatsuki-Horimoto K, Fukuyama S, Takashita E, Ozawa M, et al. A novel bivalent vaccine based on a PB2-knockout influenza virus protects mice from pandemic H1N1 and highly pathogenic H5N1 virus challenges. J Virol 2013;87(July (14)):7874–81.
[26] Kida H, Brown LE, Webster RG. Biological activity of monoclonal antibodies to operationally defined antigenic regions on the hemagglutinin molecule of A/Seal/Massachusetts/1/80 (H7N7) influenza virus. Virology 1982;122(October (1)):38–47.
[27] Das SC, Hatta M, Wilker PR, Myc A, Hamouda T, Neumann G, et al. Nanoemulsion W805EC improves immune responses upon intranasal delivery of an inactivated pandemic H1N1 influenza vaccine. Vaccine 2012;30(November (48)):6871–7.
[28] Jia N, Wang SX, Liu YX, Zhang PH, Zuo SQ, Lin Z, et al. Increased sensitivity for detecting avian influenza-specific antibodies by a modified hemagglutination inhibition assay using horse erythrocytes. J Virol Methods 2008;153(October (1)):43–8.
[29] Kayali G, Setterquist SF, Capuano AW, Myers KP, Gill JS, Gray GC. Testing human sera for antibodies against avian influenza viruses: horse RBC hemagglutination inhibition vs. microneutralization assays. J Clin Virol 2008;43(September (1)):73–8.
[30] Clements ML, Betts RF, Tierney EL, Murphy BR. Serum and nasal wash antibodies associated with resistance to experimental challenge with influenza A wild-type virus. J Clin Microbiol 1986;24(July (1)):157–60.
[31] Benton KA, Misplon JA, Lo CY, Brutkiewicz RR, Prasad SA, Epstein SL. Heterosubtypic immunity to influenza A virus in mice lacking IgA, all Ig, NKT cells, or gamma delta T cells. J Immunol 2001;166(June (12)):7437–45.
[32] Shio MT, Kassa FA, Bellemare MJ, Olivier M. Innate inflammatory response to the malarial pigment hemozoin. Microbes Infect 2010;12(November (12–13)): 889–99.